Coenzyme A governs proinflammatory macrophage metabolism

Greg. A. Timblin[1,10], Kevin. M. Tharp[1], Johanna ten Hoeve[2], Ilayda Baydemir[3], Chandra Khantwal[4], Joshua N. Farahzad[5], Jorge Domínguez-Andrés[3], Russell E. Vance[6-8], Valerie M. Weaver[1,9,10]

[1]Center for Bioengineering and Tissue Regeneration, Department of Surgery, University of California San Francisco, San Francisco, CA 94143, USA

[2]UCLA Metabolomics Center, Department of Molecular and Medical Pharmacology, University of California, Los Angeles, Los Angeles, CA, USA

[3]Department of Internal Medicine and Radboud Institute for Molecular Life Sciences (RIMLS), Radboud University Medical Center, 6525 GA Nijmegen, The Netherlands.

[4]MuriGenics Inc., 941 Railroad Ave Vallejo, CA 94592, USA

[5]Inapill, Inc., Berkeley, CA, 94709, USA

[6]Division of Immunology and Pathogenesis, Department of Molecular and Cell Biology, University of California, Berkeley, CA, USA.

[7]Cancer Research Laboratory and the Immunotherapeutics and Vaccine Research Initiative, University of California, Berkeley, CA, USA.

[8]Howard Hughes Medical Institute, University of California, Berkeley, CA, USA.

[9]Department of Bioengineering and Therapeutic Sciences and Department of Radiation Oncology, Eli and Edythe Broad Center of Regeneration Medicine and Stem Cell Research, and The Helen Diller Family Comprehensive Cancer Center, University of California San Francisco, San Francisco, CA 94143, USA.

[10]co-corresponding author*

*correspondence: valerie.weaver@ucsf.edu and greg.timblin@ucsf.edu

Abstract

The magnitude and duration of Toll-like receptor (TLR)-dependent macrophage proinflammatory responses are tightly regulated. Chronic TLR signaling drives tolerance, an immunosuppressed state of innate immune memory. Understanding of this regulation is incomplete. Here, we demonstrate that direct Coenzyme A (CoA) supplementation both reverses tolerance, and enhances TLR-dependent macrophage proinflammatory responses. Synergizing with TLR-driven glycolysis, CoA enhances glucose entry into the mitochondrial TCA cycle, fueling acetyl-CoA and citrate biosynthesis for epigenetic activation of proinflammatory gene transcription. CoA unlocks tumor-associated macrophage (TAM)-dependent TLR agonist anti-tumor activity in breast cancer, and promotes macrophage restriction of the intracellular bacterial pathogen *Legionella pneumophila*. Our findings identify CoA-dependent mitochondrial glucose utilization, and not aerobic glycolysis, as the key metabolic flux supporting TLR-dependent macrophage proinflammatory responses. Moreover, they show tolerance is a plastic state amenable to reversal by CoA, which re-routes glucose to restore requisite metabolic support of said responses, reversing myeloid immunosuppression in cancer and infection.

Introduction

Macrophage Toll-like receptor (TLR)-dependent proinflammatory responses to pattern-and damage-associated molecular patterns (PAMPs, DAMPs) are crucial for anti-tumor and anti-pathogen immunity, as well as initiating inflammation following tissue injury (*1*). Tolerance, a form of innate immune memory whereby macrophages chronically exposed to PAMPs/DAMPs enter an immunosuppressed state and are refractory to TLR restimulation (*2*), both suppresses proinflammatory responses to protect the host from collateral damage, and activates pro-resolving, wound healing programs necessary for tissue repair at infection/injury sites (*3–8*). However, this immunosuppressed state can work against the host in cancer and sepsis, particularly if the initial inflammatory threat (i.e. transformed cells, pathogen) is not eliminated, or new threats (i.e. metastatic lesions, opportunistic secondary infections) present themselves (*9–12*). An improved mechanistic understanding of tolerance is needed to design strategies for reversing myeloid immunosuppression in these settings for therapeutic benefit.

Immunosuppressed patient myeloid cells display bioenergetic defects (*13*), warranting deeper knowledge of how cellular metabolism supports or restricts proinflammatory programing. Macrophage proinflammatory responses, and subsequent tolerance to the TLR4 ligand lipopolysaccharide (LPS), represents a clinically-relevant and intensively studied model where links between metabolism and proinflammatory programming have been investigated. Early work suggested that attenuation of mitochondrial oxidative phosphorylation (mitoOXPHOS) and electron transport chain (ETC) activity, Tricarboxylic Acid (TCA) cycle dysfunction/metabolite accumulation, and a switch to aerobic glycolysis where glucose is converted to lactate, supported macrophage proinflammatory response to LPS (*14*). However, subsequent reports assessing metabolic requirements for proinflammatory responses over time have revealed critical cooperation between glycolysis and mitochondrial oxidative metabolism during the early acute stage. Namely, within minutes/hours following LPS stimulation, the biosynthetic function of the mitochondrial TCA cycle is crucial for utilizing glucose-derived carbons from glycolysis to produce the acetyl-CoA and citrate that epigenetically support proinflammatory gene transcription via histone acetylation (*15*,

16). Furthermore, following this rapid oxidative burst, the aforementioned shutdown of mitochondrial oxidative metabolism serves to starve the anabolic demands of the proinflammatory response, preventing sustained and future proinflammatory responses via tolerance (*15*, *17*). Concurrently, a switch to aerobic glycolysis results in lactate production, which epigenetically promotes the transition to an immunosuppressive, tissue repair/wound-healing macrophage phenotype via histone lactylation (*6*, *7*, *18*). Collectively, these findings suggest a role for the rewiring of glucose metabolism in macrophage tolerance. The precise regulators, and whether restoring glucose flux into the TCA cycle might reverse aspects of macrophage tolerance, are unclear.

Coenzyme A (CoA) is a Vitamin B5-derived coenzyme involved in numerous intracellular metabolic pathways. Here, we uncover a critical, limiting role for CoA in TLR-dependent macrophage proinflammatory responses. We find direct CoA supplementation synergizes with TLR signaling to both reverse tolerance, and enhance the magnitude of macrophage proinflammatory responses. Cooperating with TLR signaling that drives glycolytic glucose oxidation, extracellular CoA taken up directly by macrophages promotes glucose entry into the mitochondrial TCA cycle to enhance acetyl-CoA and citrate production, supporting enhanced proinflammatory gene transcription. Thus, effective levels of CoA in macrophages govern glucose fate, and in turn, the magnitude of TLR-dependent proinflammatory responses. These findings reveal that macrophage tolerance is a plastic state amenable to reversal via CoA-dependent re-routing of glucose utilization. Moreover, the data demonstrate proof-of-concept that CoA-driven metabolic rewiring holds promise in reversing myeloid immunosuppression in cancer and infection.

CoA reverses tolerance and enhances TLR-dependent proinflammatory responses *in vitro* and *in vivo*

Having found that CoA supplementation restored LPS-dependent proinflammatory gene transcription in macrophages treated with various anti-inflammatory small molecules (*17*), we hypothesized that CoA might reverse LPS tolerance in primary murine bone-marrow derived macrophages (BMDMs). Consistently, CoA supplementation (2.5mM, in line with intramitochondrial concentrations (*19*)) was

sufficient to elevate proinflammatory transcript levels in tolerized BMDMs (Fig. 1A). Moreover, CoA synergized with LPS to partially or completely restore induction of genes encoding proinflammatory cytokines (*Il1b*, *Il12b*, *Il6*) and *Nos2* (encoding inducible nitric oxide synthase, which generates tumoricidal/microbicidal NO) in tolerized BMDMs to levels observed in naïve BMDMs (Fig. 1A). *Tnf* tolerance was unaffected (Fig. S1A).

Given the effects on tolerance, we hypothesized that CoA might enhance LPS-dependent proinflammatory responses in naïve macrophages. Indeed, BMDM CoA supplementation, which alone was sufficient to upregulate proinflammatory transcript levels, strongly synergized with LPS to enhance proinflammatory transcriptional output (Fig. 1B, 250-500μM CoA, in line with average intracellular concentrations (*19*)). CoA synergy with LPS was also observed in RAW 264.7 macrophages and THP-1 monocytic cells (Fig. 1B). *Tnf* induction was unaffected (Fig. S1B). CoA's immunostimulatory effects extended to primary human myeloid cells, as CoA dose-dependently enhanced *IL1B*, *IL1A*, *IL6*, and *TNF* expression in donor monocytes either alone, or in combination with LPS (Fig. S1C).

As *in vivo* murine proinflammatory responses to LPS are largely macrophage-dependent (*20*, *21*), we tested if CoA enhanced this response. CoA alone showed little proinflammatory activity in naïve mice (Fig. 1C). However, levels of nearly two-thirds of the LPS-induced proinflammatory cytokines, chemokines, and growth factors quantified were significantly enhanced by CoA/LPS co-administration versus LPS alone (Fig. 1C). CoA/LPS also significantly enhanced the induction of anti-inflammatory and Type 2 cytokines (e.g. IL-10, IL-4, IL-13) coordinately upregulated with proinflammatory mediators by LPS to ensure the proinflammatory response is appropriately resolved and shifted to a tissue repair phase (Fig. S1D). This suggests CoA augments all (and not selective) aspects of an *in vivo* LPS-driven proinflammatory response. Together, these studies demonstrate the ability of CoA to reverse aspects of tolerance, and enhance LPS-driven proinflammatory responses *in vitro* and *in vivo*.

CoA enhances glucose entry into the mitochondrial TCA cycle

CoA's synergy with LPS on timescales relevant for proinflammatory gene induction led us to hypothesize that CoA was enhancing some aspect of metabolism

critical for TLR-dependent proinflammatory gene transcription. Given the aforementioned importance of glucose, a competitive labeling strategy using ^{13}C6-glucose isotope tracing was employed to assess differences in metabolic pathway activity in 4-hydroxyestrone (4-OHE1)-pretreated, LPS-stimulated macrophages without or with CoA supplementation. Our previous work showed that 4-OHE1 causes mitochondrial oxidative stress, depleting CoA and acetyl-CoA to significantly impair LPS-induced histone acetylation, with minimal effects on LPS-induced NFκB DNA binding (*17*) (Fig. 2A). CoA overcomes the anti-inflammatory effects of 4-OHE1, rescuing LPS-induced gene expression to levels even beyond that in macrophages treated with LPS alone (Fig. 2A). Following pretreatments and LPS stimulation, ^{13}C6-glucose was provided to macrophages for the final 30 minutes of a 1.5 hour LPS stimulation (Fig. 2B). Metabolite extraction and liquid chromatography/mass spectrometry (LC/MS) metabolomics were performed, and the relative fractional contribution (FC) of ^{13}C6-glucose to approximately 130 different intracellular metabolites was quantified. Interestingly, while CoA supplementation had no discernable effects on the labeling of glycolytic intermediates between conditions, the ^{13}C6-glucose FC to nearly all TCA cycle metabolites was significantly enhanced by CoA supplementation (Fig. 2B). Acetyl-CoA supplementation, which we showed also rescued *Il1b* repression by 4-OHE1 (*17*), phenocopied this effect (Fig. 2B), implying CoA is the active moiety of acetyl-CoA. The enhanced ^{13}C6-glucose labeling was particularly noticeable for acetyl-CoA and citrate (Fig. S2A), and occurred independent of accumulation of citrate (Fig. S2B), consistent citrate consumption for anabolic processes. Mitochondrial glucose utilization is critical for macrophage proinflammatory responses via supplying the acetyl-CoA and citrate to fuel epigenetic activation of LPS-induced proinflammatory genes via histone acetylation (*15*, *16*). These results suggest CoA's enhancement of glucose entry into the mitochondrial TCA cycle, which fuels metabolic-epigenetic support of proinflammatory gene transcription, underlie its proinflammatory and tolerance-reversing effects.

Further supporting this hypothesis, in naïve macrophages, CoA alone was sufficient to enhance ^{13}C6-glucose FC to TCA cycle metabolites. Compared to LPS, CoA drove relatively less ^{13}C6-glucose FC to metabolites in upper glycolysis and

offshoots where LPS has been previously shown to enhance labeling (*22*) (Fig. S2C). Such "priming" of the TCA cycle could explain both the ability of CoA alone to upregulate proinflammatory gene expression in the absence of exogenously added TLR ligands, and the observed synergy between CoA and LPS. In tolerized macrophages, while secondary LPS stimulation further promoted ^{13}C6-glucose labeling of lactate, CoA supplementation had exactly the opposite effect, increasing unlabeled m0 lactate and reducing m+3 lactate (Fig. S2D). This coincided with a decrease in total lactate levels in tolerized macrophages treated with CoA (Fig. S2D), suggesting CoA promotes an alternative glucose fate. Indeed, CoA concurrently enhanced ^{13}C6-glucose entry into the TCA cycle both via malic enzyme (ME)- and pyruvate carboxylase (PC)-mediated reductive carboxylation of pyruvate (indicated by increased m+3 malate and m+3 oxaloacetate), and via pyruvate dehydrogenase (PDH) as indicated by increased m+5 citrate (i.e. citrate formed via condensation of m+2 acetyl-CoA with m+3 oxaloacetate) (Fig. S2D). This suggests CoA's promotion of glucose anaplerosis via ME and PC (which is allosterically activated by acetyl-CoA (*23*)) replenishes a broken TCA cycle to support citrate biosynthesis in the face of known downstream TCA impediments in tolerized macrophages (e.g. IRG1-promoted extraction of carbons from the cycle for itaconate synthesis, NO-mediated inhibition of aconitase (*24*), itaconate inhibition of succinate dehydrogenase (*25*), etc.). It also suggests CoA re-invigorates some level of PDH activity despite reduced PDH lipoylation, and oxidative-/NO-mediated damage to PDH, that occurs following primary LPS stimulation (*24*, *26*). Collectively, these results across experimental models support the hypothesis that CoA enhances macrophage proinflammatory responses and reverses tolerance, at least in part, by promoting glucose entry into the mitochondrial TCA cycle.

CoA enhances macrophage-dependent TLR agonist anti-tumor activity and macrophage anti-microbial activity

We next tested whether CoA supplementation could improve outcomes in situations where macrophage tolerance contributes to impaired host defense. The use of immunostimulatory agents such as TLR agonists to reprogram tumor-associated macrophages (TAMs) to a proinflammatory phenotype that supports anti-tumor

immunity has been extensively studied (*27*), but with mixed clinical success (*28*). The ineffectiveness of TLR agonists as monotherapies may lie in tolerance. Similarities have been noted between tolerized macrophages and immunosuppressive TAMs (*29–31*), suggesting DAMPs released from stressed/dying cells in the tumor microenvironment (TME) chronically condition TAMs towards tolerance (*32*). Breast cancer TAMs are a potent source of TGFβ (*33*), a hallmark cytokine of tolerized macrophages (*5*). Moreover, TAMs isolated from spontaneous MMTV-PyMT breast tumors display tolerance, as the TLR4 agonist monophosphoryl Lipid A (MPLA, a LPS derivative and clinically-approved vaccine adjuvant) is unable to upregulate proinflammatory genes involved in anti-tumor immunity *in vitro,* or slow tumor growth *in vivo*, unless combined with IFNγ (*12*). Interestingly, CoA's effects described thus far in many ways phenocopy IFNγ (a.k.a. "macrophage-activating factor"), a cytokine known to potentiate LPS-dependent macrophage proinflammatory responses (often called "priming") (*34*, *35*), reverse macrophage tolerance (*36–39*), and promote macrophage anti-tumor activity (*40*, *41*). These findings led us to hypothesize that CoA co-administration with MPLA would unlock the anti-tumor activity of this TLR agonist.

Similar to other tumor models (*12*, *42*, *43*), intratumoral (i.t) MPLA alone had no effect on MMTV-PyMT orthotopic breast tumor growth (Fig. 3A left, Fig. S3A). However, an MPLA+CoA combination therapy significantly slowed tumor growth (Fig. 3A left, Fig. S3A), phenocopying MPLA+IFNγ (Fig. 3A right, Fig. S3A). Interestingly, CoA alone had a measurable effect on tumor growth (Fig. 3A left, Fig. S3A), suggesting CoA helps TAMs overcome tolerance and mount proinflammatory responses to endogenous DAMPs. In support of this, both CoA monotherapy, and MPLA+CoA, were superior to MPLA monotherapy at elevating i.t. proinflammatory gene expression and cytokine levels (Fig. 3B). These measurements were made 16 hours after the final i.t. therapy injection, a timepoint when an acute inflammatory response would have resolved, suggesting CoA helps TAMs mount sustained proinflammatory responses to endogenous DAMPs and/or MPLA. The anti-tumor effects of the MPLA+CoA combination therapy was dependent on TAMs, as their depletion abrogated its ability to slow tumor growth (Fig. S3B-D). Together, these results support the proposed

hypothesis, and suggest that CoA-dependent tolerance reversal improves efficacy of TLR agonist immunotherapy via enabling TAM proinflammatory reprogramming.

Evidence suggest that tolerance contributes to host immunosuppression during infection, particularly with pathogens that replicate within macrophages. Intracellular bacterial pathogens generally suppress macrophage mitoOXPHOS, shifting host metabolism towards aerobic glycolysis (*44*), the metabolic program of tolerance. This suggests TLR signaling triggered by PAMPs, pathogen effectors that disrupt mitoOXPHOS (*45*), or both, promote aerobic glycolysis to create a tolerized replicative niche. IFNγ enhances macrophage anti-microbial activity (*46*, *47*) via induction of host genes that restrict intracellular pathogen growth, with full induction of restriction genes like *Nos2* requiring synergy between IFNγ and TLR signaling (*40*). Thus, IFNγ's restrictive effects may lie in its ability to reverse tolerance and enable full expression of host restriction genes. Given CoA's ability to redirect glucose into the mitochondrial TCA cycle and reverse tolerance, we hypothesized that CoA would phenocopy IFNγ in restricting intracellular pathogen replication in macrophages.

To test this, we utilized *Legionella pneumophila*, a gram-negative intracellular bacterial pathogen and causative agent of a severe type of pneumonia, Legionnaires' Disease. During macrophage infection, *L. pneumophila* triggers multiple TLRs (*48*), and secretes multiple effectors that cause mitochondrial stress and suppress mitoOXPHOS (*49–51*). This diverts host metabolism towards aerobic glycolysis (*49*), indicative of tolerance. IFNγ potently restricts *L. pneumophila* intracellular replication in a manner that depends in part on host induction of *Nos2* and *Irg1* (*52*). *Nos2* and *Irg1* were induced in uninfected BMDMs by CoA alone, and induction was further enhanced with CoA/LPS cotreatment (Fig. S3E). To track *L. pneumophila* replication in host macrophages, we used a previously validated luminescent strain (*53*, *54*). *L. pneumophila* flagellin potently triggers macrophage pyroptosis, so to avoid this confounding effect, we used a flagellin-deficient (Δ*flaA*) luminescent strain (*53*, *54*). Real-time tracking demonstrated robust Δ*flaA L. pneumophila* replication in BMDMs (Fig. 3C). However, CoA supplementation restricted growth in a dose-dependent manner (Fig. 3C left), phenocopying IFNγ (Fig. 3C right). CoA-mediated restriction, which was confirmed at the level of bacteria colony-forming units (CFUs, Fig. S3F),

occurred independent of direct effects on *L. pneumophila* growth or luminescence (Fig. S3G), or BMDM viability (Fig. S3H). These results demonstrate that CoA promotes a proinflammatory, anti-microbial macrophage phenotype and restricts intracellular pathogen growth, potentially through overcoming microbe-driven metabolic reprogramming and tolerance.

CoA's enhancement of proinflammatory gene transcription requires direct CoA uptake and TLR signaling

We next investigated how exogenous CoA positively influenced glucose entry into a CoA-dependent intracellular metabolic pathway. The extracellularly-generated CoA degradation products 4-phosphopantetheine (PPanSH) and pantothenate (Pan, Vitamin B5) can enter cells and feed the endogenous CoA biosynthesis pathway (*55*, *56*)(Fig. 4A). We detected increased PPanSH, but not Pan, within macrophages supplemented with CoA, and within tumors receiving i.t. CoA (Fig. S4A). However, neither PPanSH or Pan supplementation phenocopied CoA's ability to upregulate basal proinflammatory gene expression in macrophages (Fig. 4B), or synergize with LPS (Fig. S4B). The CoA degradation products adenosine 3',5' diphosphate and dephospho-CoA also lacked these activities (Fig. 4B, Fig. S4B). Thus, no extracellularly-generated CoA degradation product phenocopied CoA's effects of macrophage proinflammatory gene transcription, suggesting macrophages take up intact extracellular CoA. In support of this, preincubation of CoA with non-heat inactivated fetal bovine serum containing active ectonucleotide pyrophosphatase/phosphodiesterase (ENPP) enzymes that degrade CoA to PPanSH (*55*) significantly abrogated CoA's ability to upregulate *Il1b* expression (Fig. 4C), an effect reversed by serum heat inactivation that kills ENPP activity. Thus, as no plasma membrane transporter or uptake mechanism from the extracellular space has been previously described for CoA (*56*), this suggests macrophages are a unique cell type capable of directly acquiring extracellular CoA from their environment to augment glucose entry into a CoA-dependent intracellular metabolic pathway.

While our data suggests synergy between CoA and TLR signaling, the exact nature of this relationship remained unclear. This synergistic relationship was particularly intriguing as CoA alone was sufficient to promote glucose entry into the TCA

cycle in BMDMs (Fig. S2C), and upregulate proinflammatory gene expression in BMDMs (Fig. 1B) and tumors (Fig. 3B), even in the absence of exogenous TLR ligands. TLR signaling via adaptor proteins, primarily MyD88 for proinflammatory genes, activates signal-dependent transcription factors (SDTFs, e.g. NFκB), which bind *cis* regulatory elements made accessible by lineage-determining transcription factors (LDTFs, e.g. PU.1)(*57*). SDTFs recruit HATs (e.g. p300) that use acetyl-CoA to activate proinflammatory gene transcription via histone acetylation (*15*, *16*). TLR signaling via MyD88 also promotes glucose uptake and glycolytic glucose oxidation (*58*) for acetyl-CoA production (*15*, *16*). BMDM cultures contain dying cells that modulate the outputs of bystander macrophages exposed to exogenous stimuli (e.g. exogenous IL-4 added to BMDMs can only activate certain tissue repair gene expression programs if apoptotic cells are present as a co-signal (*59*)). As stressed/dying cells release DAMPs that trigger TLRs, we reasoned that DAMPs trigger a basal level of tonic TLR signaling in BMDMs that drives glycolytic glucose oxidation. In support of this concept, *Myd88*$^{-/-}$ BMDMs display decreased basal glucose uptake and glycolysis compared to WT BMDMs even in the absence of exogenous TLR ligands (*16*). Thus, we hypothesized that the ability of CoA to enhance proinflammatory gene transcription might be dependent on TLR signaling, which provides 1) glucose-derived carbons from MyD88-driven glycolysis for CoA to route into the mitochondrial TCA cycle, and 2) SDTF activation.

To test this, we utilized BMDMs from *Tlr2*$^{-/-}$ *Tlr4*$^{-/-}$ *Unc93b1*$^{-/-}$ mice (*60*), henceforth referred to as TLR KO BMDMs. TLR KO BMDMs displayed reduced basal expression of *Il1b*, *Il6*, but not *Tnf*, in the absence of exogenously added TLR ligands (Fig S4C.). Indeed, the proinflammatory effects of CoA were significantly reduced in TLR KO BMDMs (<1% of the *Il1b* fold induction observed in WT BMDMs), which lack the ability to respond to exogenous TLR ligands (Fig. 4D). Thus, CoA's ability to upregulate proinflammatory gene transcription is largely TLR-dependent.

We next reasoned that if CoA's ability to upregulate proinflammatory gene expression was dependent on MyD88-driven glycolysis and SDTF activation, then CoA should synergize with other MyD88-activating signals to enhance proinflammatory gene transcription. Like TLRs, the Interleukin 1 receptor (IL-1R) signals via MyD88 to

upregulate proinflammatory gene expression in response to IL-1 cytokines. Indeed, we found that CoA synergized with exogenously added recombinant IL-1β to significantly upregulate proinflammatory gene transcription in TLR KO BMDMs (Fig. 4E). This result further supports a model in which the proinflammatory effects of CoA lie in its ability to synergize with MyD88-driven glycolytic glucose oxidation to route glucose-derived carbon into the mitochondrial TCA cycle for acetyl-CoA and citrate biosynthesis that, in cooperation with MyD88-activated SDTFs, epigenetically supports proinflammatory gene transcription (Fig. 4F).

Discussion

Our findings here define CoA as an absolutely critical, limiting input for TLR-dependent macrophage proinflammatory responses. Moreover, they demonstrate that tolerance, an immunosuppressed state of innate immune memory driven by chronic TLR signaling, is plastic and partially reversible via direct CoA supplementation, which works downstream of TLR-driven glycolysis to enhance glucose entry into the mitochondrial TCA cycle, restoring metabolic-epigenetic support of macrophage proinflammatory gene transcription. Our results also suggest macrophages are the first described cell type capable of directly acquiring CoA from their extracellular environment to support intracellular CoA-dependent metabolic pathways. Thus, together with our previous work showing the potent anti-inflammatory effects of CoA depletion (*17*), our work demonstrates that effective CoA levels in macrophages governs the glucose utilization necessary for metabolic support of TLR-dependent macrophage proinflammatory responses.

Proinflammatory responses are massively anabolic processes requiring glucose for producing metabolites for epigenetic activation of proinflammatory genes, nucleotides for transcription of highly-induced mRNAs, and proteins/lipids/sugars for proinflammatory mediator secretion. In yeast and other mammalian cells, glucose levels and glycolysis are inexorably linked to acetyl-CoA levels, with growth factor signaling having evolved in higher organism as additional an promoter of glucose uptake and utilization. In turn, high acetyl-CoA is indicative of “fed” state where the anabolic processes of growth and proliferation are licensed to proceed via histone acetylation

and transcriptional activation of surprisingly specific, glucose-responsive, growth-promoting gene expression programs (*61–64*). Thinking of macrophages collectively as a specialized tissue whose job is not to proliferate in response immunostimulatory PAMPs/DAMPs (which can be thought of as “growth factors”), but rather to produce massive amounts of proinflammatory mRNAs, proteins, lipids, etc., it is logical that glucose availability, glucose utilization, and acetyl-CoA levels would be tightly linked to proinflammatory transcriptional programs in these cells, as they can only engage said programs if the requisite fuel is present. Indeed, myeloid cells are responsive to glucose concentrations, with high glucose being sufficient to upregulate proinflammatory gene histone acetylation and transcription (*65*, *66*). Our work demonstrates CoA, not a nutrient itself, but rather a key facilitator of glucose utilization that routes glucose carbons into metabolites required for activation of proinflammatory genes, is sufficient to activate proinflammatory transcription programs, as long as some level of TLR-dependent “growth factor” signaling is present to promote glucose uptake and glycolytic oxidation. Moreover, CoA has the ability to overcome the evolved rewiring of glucose metabolism in tolerance that acts to suppress proinflammatory transcriptional programs, restoring anabolic glucose utilization that support proinflammatory responses in immunosuppressed myeloid cells.

Immune suppression is a barrier to the treatment of inflammatory diseases, including cancer and sepsis, because both sterile and non-sterile PAMP/DAMP-triggered inflammation have evolved strong negative feedback mechanisms to resolve inflammation, which both protects the host, and transitions responses to an injury-reparative phase. In solid tumors such as breast cancer, this response protects and promotes tumor growth, with TAMs polarizing towards a wound-healing, TGFβ-producing, pro-resolution phenotype. These TAMs promote tumor fibrosis via activation of stromal cells (*33*), and acquisition of a collagen-biosynthetic, immunosuppressive phenotype (*67*). The nutrient fluxes in theses TAM are likely incompatible with the fluxes supporting a proinflammatory phenotype, as the biosynthetic goals of these macrophages (collagen production for repair vs. proinflammatory mediator production for defense) are divergent. While TAMs are copious consumers of glucose in the TME (*68*), if the flux of this glucose is more directed towards lactate (supports pro-resolving

phenotype) or serine (supports collagen biosynthesis) versus the mitochondrial TCA cycle, this would be counterproductive to proinflammatory responses, and consistent with the aforementioned TAM tolerance phenotype (*12*). In turn, failures of therapies aimed at reprograming TAMs to a proinflammatory phenotype may lie in failure to overcome the barrier that is the metabolic programming that enforces tolerance. Simply providing an proinflammatory signal is likely insufficient for TAM reprogramming, as it doesn't overcome said barrier, nor does it assist TAMs in engaging the metabolic fluxes that support proinflammatory gene expression. Our work combining MPLA with CoA represents proof-of-concept that combining an immunostimulatory cue with a factor promoting specific aspects of macrophage glucose metabolism critical for proinflammatory responses can improve TAM-targeted immunotherapy efficacy. Our results also suggest CoA supplementation, given its similarity to the clinically used immunostimulatory agent in IFNγ, may have promise in reinvigorating host immunity in other settings. For example, CoA's ability to promote macrophage *L. pneumophila* restriction implies it may have utility as an immunostimulatory therapy in chronic infections associated with immunosuppression (e.g. *Mtb* infection), or in sepsis-associated immune suppression that often results in secondary infections (and shares many parallels with cancer-associated immunosuppression (*11*)). Aging is associated with reduced mitochondrial respiratory capacity, which coincides with myeloid immunosuppression, increased cancer incidence, increased susceptibility to infections, poor sepsis outcomes, and impaired responses to vaccination. Whether CoA is capable of combating innate immune decline in aging by reinvigorating proinflammatory responses in aged myeloid cells is also worth investigating.

How extracellular CoA is taken up by macrophages to positively influence CoA-dependent glucose utilization is unclear, as there is no described plasma membrane transporter or uptake mechanism (*56*). Moreover, that extracellular CoA is proinflammatory raises the possibility that CoA released into the extracellular space during tissue damage represents a previously unappreciated mitochondrial DAMP (*1*) that acts to promote sterile inflammation not via stimulating TLRs or other receptors, but instead by augmenting specific aspects of macrophage metabolism that support proinflammatory gene expression. If true, our data suggests degradation by ENPPs

works against CoA's proinflammatory effects, and would antagonize CoA-driven inflammation following injury. This would be analogous to how other immunostimulatory molecules released in damaged/disorganized tissues (e.g. wounds, tumors), such as ATP released from injured/dying cells, and cyclic dinucleotides produced by the cGAS-STING pathway following self-nucleic acid mislocalization, are degraded by ENPPs to resolve inflammation, but work against productive anti-tumor immunity (*69*).

Methods

Animals

All experiments were approved by the UCSF Institutional Animal Care & Use Committee (IACUC) to ensure ethical use of animals (Protocol AN194983-01), and performed under the supervision of the UCSF Laboratory Animal Resource Center (LARC). C57BL/6J mice (strain #000664) were purchased from Jackson Labs. TLR KO mice were generous gift from Dr. Greg Barton (UC Berkeley). Animals were housed under standard conditions (20-23°C, 50% humidity, 12h/12h light/dark cycle).

Cell culture

For all experiments except *L. pneumophila* infection model, bone marrow-derived macrophages (BMDMs) were prepared from 6-12-week-old female C57BL/6J mice by plating bone marrow in DMEM (GeneClone 25-500) supplemented with 10% fetal bovine serum (FBS, HyClone SH30071.03m, non-heat inactivated), penicillin/streptomycin (Gibco 15140-122), and 20ng/mL recombinant murine M-CSF (Shenandoah 200-08 or BioLegend 576404) in non-TC treated Petri dishes, refreshing media every 3 days. Cells were harvested by lifting with PBS with 4mM EDTA with gentle scraping, and plated in TC-treated 24-well plates at 1 x 10^5 cells per well on days 6-10. For experiments looking solely at naïve macrophage LPS responses, 100 ng/mL LPS was used. BMDM tolerance was induced by stimulating naïve BMDMs for 24 hours with 100 ng/mL LPS (Sigma L3024). Following a media change and 2 hour recovery period, tolerized and control naïve macrophages were (re)stimulated with 10 ng/mL LPS. For CoA pre-incubation experiments, FBS heat-inactivation was carried out by

incubating HyClone SH30071.03m at 56°C for 30 minutes. Then,1 part CoA was mixed with 9 parts PBS, media, non-heat-inactivated FBS, or heat-inactivated FBS, in a 1.5mL tube and incubated at 37°C for 3h. Afterwards, the entirety of each tube was added to BMDMs.

For *L. pneumophila* infection experiments, BMDMs were prepared by plating bone marrow in RPMI (Gibco 21870-076) supplemented with 2mM glutamine (Gibco 25030081), 10% FBS (Gibco 16140-071, heat inactivated), and 5% supernatant from 3T3 cells expressing macrophage colony-stimulating factor (generated in-house in Vance Lab). RAW 264.7 macrophages were cultured in DMEM with 10% FBS and pen/strep. THP-1 cells were cultured in RPMI 1640 (GeneClone 25-506) supplemented with 10% FBS and pen/strep (both from ATCC via the UC Berkeley Cell Culture Facility). MMTV-PyMT breast cancer cell line was cultured in 50/50 mix of DMEM and F12 (Gibco 11765-054) with 10% FBS and pen/strep.

Chemicals

Coenzyme A (CoA) used in the majority of experiments was from CoALA (CA02, lithium salt), though we confirmed CoA from two other sources (Sigma C4780, Cayman 16147) produced similar results *in vitro*. Sigma CoA was also used in the *in vivo* LPS challenge experiment, and in the metabolomics in Figure 2B. (Figure S2C, S2D metabolomics used CoALA CoA). Acetyl-CoA (A2056), Pantothenate/Vitamin B5 (21210), LPS (L3024) and poly IC (P0913) were from Sigma. 3'-dephosphoCoA (27390) and adenosine 3',5'-diphosphate (24265) were from Cayman. 4-phosphopantetheine (CX11340) was from Chiralix. MPLA (tlrl-mpls), Pam3CSK4 (tlrl-pms) and ODN (tlr1-1826-1) were from InvivoGen. Recombinant murine IFNγ was from PeproTech (315-05) or BioLegend (575304). Recombinant murine IL-1β was from BioLegend (575102).

Quantitative real-time PCR (qPCR) for gene expression

Cells were lysed in Trizol (Invitrogen) and total RNA isolated via chloroform extraction according to manufacturer's instructions using GlycoBlue (AM9515) to assist RNA precipitation. cDNA was prepared from approximately 250ng of total RNA with random hexamer priming using M-MLV Reverse Transcriptase (BioChain Z5040002-

100K). qPCR was performed on an Eppendorf Mastercycler Realplex2 epgradient S qPCR machine using PerfeCTaSYBR Green FastMix (Quantabio 95072-05K). Primers (IDT) were designed to amplify exon-spanning sequences in target mRNAs using Primer-BLAST. All data is normalized to *Hprt* expression using the delta-delta Ct method.

Primer sequences (5'-3' F, 5'-3' R):

Mouse

Hprt - TCAGTCAACGGGGGACATAAA, GGGGCTGTACTGCTTAACCAG

Il1b - CGTGGACCTTCCAGGATGAG, CGTCACACACCAGCAGGTTA

Il1a - AACGTCAAGCAACGGGAAGA, GCTGATCTGGGTTGGATGGT

Il6 – CGATAGTCAATTCCAGAAACCGC, TGGTTGTCACCAGCATCAGTC

Tnf - CCCTCACACTCAGATCATCTTCT, GCTACGACGTGGGCTACAG

Il12b - TCTCCTGGTTTGCCATCGTT, GGGAGTCCAGTCCACCTCTA

Nos2 - GTTCTCAGCCCAACAATACAAGA, GTGGACGGGTCGATGTCAC

Irg1 - AGCAACTACTCCTGCCATCC, CAAGCCGTGAATCATACCAGC

Cybb - TGCTAACATGGGGAACTGGG, AGAGGAAGACATTCAGCCCC

Casp4 - TAGGCTACGATGTGGTGGTG, TGCTGTCTGATGTCTGGTGT

Irgm1 - CAGCCCAAACCGTAGAGGAC, CGAGCTGAACTGCTCAGAGG

Irgm3 - CTGAGCCTGGATTGCAGCTTT, TGAACTCTGTGGGTCTGCTCTA

Human

HPRT - TGCTGAGGATTTGGAAAGGGT, GGGCTACAATGTGATGGCCT

IL1B - GCAGCCATGGCAGAAGTACC, TGTTTAGGGCCATCAGCTTCAA

IL1A - CGGTTGAGTTTAAGCCAATCCAT, AAGGTGCTGACCTAGGCTTG

IL6 - AGTCCTGATCCAGTTCCTGC, CAGGCTGGCATTTGTGGTTG

TNF - CTGCACTTTGGAGTGATCGG, TGTCACTCGGGGTTCGAGA

NOS2 – TCTCAAGGCACAGGTCTCTTC, CAGATGTTCTTCACTGTGGGG

Monocyte isolation and stimulation

PBMC isolation was performed by differential density centrifugation over Ficoll-Paque (GE Healthcare). Percoll isolation of monocytes was performed as previously described

(*70*). Briefly, 150-200 x 10^6 PBMCs were layered on top of a hyper-osmotic Percoll solution and centrifuged for 15 min at 580g. The interphase layer was isolated and cells were washed with cold PBS. Cells were re-suspended in RPMI medium Dutch modified (Invitrogen) supplemented with 50 µg/mL gentamicin, 2 mM Glutamax, and 1 mM pyruvate, and counted. An extra purification step was added by adhering Percoll-isolated monocytes to polystyrene flat bottom plates (Corning) for 1 h at 37˚C; a washing step with warm PBS was then performed to yield maximal purity. 10^5 monocytes were added to flat-bottom 96-well plates (Greiner). Cells were stimulated with RPMI or Escherichia coli LPS (Sigma-Aldrich) at a concentration of 10 ng/mL for 4h-incubation at 37˚C. In the specific conditions described, CoA was supplemented at two doses (low: 500µM CoA, high: 5mM) 2 hours prior to LPS stimulation. Total RNA was prepared using NucleoSpin RNA Plus Mini kit (Macherey-Nagel) according to manufacturer's instructions for cDNA synthesis and qPCR as described above.

***In vivo* LPS challenge and serum cytokine array**

8 week-old male C57BL/6 mice (Envigo, 5 mice per group) were injected intraperitoneally (i.p.) with either PBS vehicle or 250 mg/kg CoA (Sigma C4780). 15 minutes later, mice were injected i.p. with either PBS vehicle or sublethal 3 mg/kg LPS dose (Sigma L2880). 4 hours later, mice were bled for serum cytokine analysis using MILLIPLEX MAP Mouse Cytokine/Chemokine Magnetic Bead Panel (Millipore MCYTOMAG-70K-PMX) according to manufacturer's instructions. One sample was excluded from the CoA/LPS group data as it was identified as an outlier by the ROUT method across multiple quantified cytokines.

PyMT breast cancer model and tumor-associated macrophage (TAM) depletion

6 week old female C57BL/6 mice were anesthetized and 250K MMTV-PyMT tumor cells (100µL total volume, 1:4 mix of cells in PBS:matrigel) injected into the inguinal fat pad near the 4th mammary gland using a 1mL syringe and 26G needle (Day 0). Palpable tumors were detectable in some animals by Day 7, and all animals by Day 10. Twice-weekly intratumoral injections were initiated on Day 11 using an insulin syringe (BD Biosciences) to deliver 50uL volumes of MPLA (1mg/tumor, DMSO vehicle), CoA (5, 50,

or 250 mg/kg, H_2O vehicle), MPLA + CoA, or vehicle controls. Tumor volumes were measured with calipers starting on Day 13 prior to injections. At experimental endpoint, mice were sacrificed and tumors excised, weighed, and either immediately processed for flow cytometry, or flash frozen, homogenized, and stored at -80°C for other uses. For TAM depletion experiment, 1mg of anti-CSF-1R (Leinco C2268) or control IgG (Leinco R1367) antibody were delivered i.p. beginning on Day 8, and MPLA + CoA treatments initiated on Day 11. Supplemental antibody injections (500ug) were given every 4-5 days through the course of the experiment to maintain TAM depletion, which was confirmed by flow cytometry.

Flow cytometry

For TAM flow cytometry, approximately 50mg of freshly excised tumor tissue was transferred to a 1.5mL tube, manually dissociated with scissors, and digested in DMEM with 0.1% collagenase (Sigma C6885) for 1.5 hour at room temperature with gentle shaking. Sample was passed through a 100μm filter, RBCs lysed, and cell pellet stained on ice in FACs buffer (PBS with 10mM HEPES and 5% BSA). After Fc Block (1:100, BD Biosciences 553142), cells were labeled with anti-CD45-PeCy7 (clone 30-F11, BD Biosciences 552848, 1:400), anti-F4/80-PE (clone BM8, eBioscience 12-4801-82, 1:200), and anti-CD11b-APC (clone M1/70, BioLegend 101225, 1:200). Cells were washed and resuspended in FACs buffer supplemented with DAPI to exclude dead cells, and live CD45+ F4/80+ CD11b+ TAMs quantified using an LSR II analyzer (BD Bioscience) running BD FACSDiva software. Data were analyzed with FlowJo (Tree Star, v10.8.1). For BMDM viability assessment after CoA supplementation, media was removed and cells washed once with PBS. Cells were then incubated in PBS with 4% EDTA supplemented with DAPI and fluorescein diacetate (FDA, Thermo Fisher F1303) at 37 ˚C for 5 min. Cells were then lifted by gentle pipetting, and the percentage of DAPI negative, FDA positive live cells per total events per well quantified using the aforementioned cytometer and software.

Intratumoral cytokines ELISA

Approximately 30mg of flash frozen, mortar and pestal-homogenized PyMT tumor tissue was transferred to an 1.5mL tube and incubated in 350uL of PBS at 37°C with shaking for 45 minutes to wash and collect intratumoral cytokines. Tumor tissue was then pelleted by centrifugation, and cytokine levels in the supernatant/PBS wash quantified using ELISA kits according to manufacturer's instructions (murine IL-1β: Invitrogen 88-7013-22, murine IL-6: Invitrogen 88-7064-88) and a SpectraMax M2 plate reader. A small number of suspected outliers were removed from some data sets using the ROUT method, leading to some discrepancies between the experimental "n" in tumor growth plots versus "n" presented in the ELISA results.

***L. pneumophila* bacterial strains and *in vitro* BMDM infection**

Δ*flaA Legionella pneumophila***,** derived from the virulent clinical isolate JR32 (*53*), were engineered to express the *Photorhabdus luminescens luxCDABE* operon as previously described (*54*). Bacteria from frozen glycerol stocks were cultured first on buffered yeast extract with charcoal (BCYE) agar plates, then in buffered yeast extract (BYE) broth supplemented with L-cysteine, ferric nitrate, and streptomycin (100ug/mL). For infection, BMDMs differentiated in RPMI/3T3 supernatant as described above were plated at 100K per well in 96-well opaque white plates in RPMI without antibiotics. The following day, BMDMs were infected with bacteria from an overnight liquid culture diluted in antibiotic-free RPMI for 1 hour at 37 ºC at a MOI of 0.01. After replacing the infection media with RPMI containing H_2O vehicle, CoA, or IFNγ (6 ng/μL), a Day 0 luminescence measurement was recorded (λ470, Spectramax L luminometer, Bio-Rad). For the 5mM CoA condition, sterile NaOH was used to correct the pH of the media, which was acidified by this high CoA concentration. Intracellular bacterial growth was then tracked over time by reading luminescence every 24 hours, with fresh CoA supplemented into the appropriate wells after each reading. At the experimental endpoint, BMDMs were lysed with water for dilution of bacteria on BYCE agar plates and enumeration of CFU.

Metabolomics

For metabolomics in Figure 2B, BMDMs were cultured in DMEM (Corning 17-207-CV) supplemented with 10% One Shot dialyzed FBS (Thermo Fisher A33820-01), 1mM sodium pyruvate (Gibco 11360-070), 4mM L-glutamine (Gibco 25030081), and 25mM glucose (Gibco A24940-01). $5x10^5$ cells were first pretreated with 250μM CoA or acetyl-CoA for 2h hours, followed by EtOH or 5μM 4-OHE1 for 1 hour. Cells were then stimulated with 100ng/mL LPS for 1.5 hours. For the last 30 minutes post-LPS stimulation, cells were washed with unsupplemented media, and provided DMEM described above except with 25mM $^{13}C_6$-glucose (Cambridge Isotope Laboratories, CLM-1396-PK) to competitively label metabolites between conditions as a proxy for metabolic pathway activity. After this 30 minutes of labeling, cells were washed with PBS and moved to dry ice for addition of 1mL ice cold 80% MeOH. Cells were incubated at -80ºC for 15 minutes, scraped on dry ice, and moved to low bind Safe-Lock 1.5mL tubes (Eppendorf cat.022363204). After centrifugation 20,000g x 10 min at 4ºC, the cell pellet was saved for protein quantification by BCA assay, while the MeOH extract was transferred to a new tube and evaporated overnight at RT using a SpeedVac. Dried extracts were stored at -80ºC. For metabolomics experiments in Figures S2C and S2D, we utilized DMEM with a lower glucose concentration (10mM, in line with RPMI glucose concentrations used for similar tracing by other groups (*15*)). This allowed better detection of LPS-induced ^{13}C6-glucose labeling of TCA cycle metabolites, potentially via reduction of basal glycolytic spillover, and/or reduction of the Crabtree effect. The media was prepared by supplementing glucose-free DMEM (Gibco 11966-25) with 10mM glucose (Gibco A24940-01) and 0.5 mM sodium pyruvate (Gibco 11360-070).

Dried MeOH extracts were resuspended in 50% ACN:water and 1/10th was loaded onto a Luna 3um NH2 100A (150 × 2.0 mm) column (Phenomenex). The chromatographic separation was performed on a Vanquish Flex (Thermo Scientific) with mobile phases A (5 mM NH4AcO pH 9.9) and B (ACN) and a flow rate of 200μL/min. A linear gradient from 15% A to 95% A over 18 min was followed by 9 min isocratic flow at 95% A and reequilibration to 15% A. Metabolites were detected with a Thermo Scientific Q Exactive mass spectrometer run with polarity switching (+3.5 kV/− 3.5 kV) in full scan

mode with an m/z range of 65-975. TraceFinder 4.1 (Thermo Scientific) was used to quantify the targeted metabolites by area under the curve using expected retention time and accurate mass measurements (< 5 ppm). Values were normalized to sample protein concentration. Relative amounts of metabolites were calculated by summing up the values for all isotopologues of a given metabolite. Fraction contributions (FC) of ^{13}C carbons to total carbon for each metabolite was calculated as previously described (*71*). Data analysis was performed using in-house R scripts available upon request.

Statistical analysis

Majority of statistical analysis was performed using GraphPad Prism 9 software. Metabolomics statistical analysis was performed using R or GraphPad Prism 9. All data were assumed to be normally distributed. One-Way ANOVA was used in initial metabolomics FC analysis comparing multiple groups, with Dunnett's post-test used to identify significant differences between specific groups. In other experiments, planned comparisons were built-in to experimental design as indicated, with Student's t-test used to make sensible comparisons between two experimental groups. Metabolomics data were log-transformed and Z-scored for representation on heatmaps. Where indicated in the methods (see above), suspected outliers were removed from experimental groups using the ROUT method.

Illustrations

Images were created using BioRender and Adobe Illustrator (licenses to G.A.T.).

Acknowledgements

We thank the following people for their helpful advice and discussion regarding the project, and/or assistance with reagents and experimentation: Dr. Kathleen Pestal (Barton Lab, UC Berkeley); Dr. Jordan Price and Kristen Witt (Vance Lab, UC Berkeley); Dr. Kelly Kersten (Krummel Lab, UCSF); Varun Bhadkamkar and Dr. Shaeri Mukherjee (USCF). This work was supported by: American Diabetes Association Postdoctoral Fellowship #1-19-PDF-058 to G.A.T.; 1F32CA236156-01A1 (NIH F32 Postdoctoral Award), 5T32CA108462-15 (NIH T32), and Sandler Program for

Breakthrough Biomedical Research (postdoctoral independence award) to K.M.T. The Netherlands Organization for Scientific Research VENI grant 09150161910024 to J.D-A. R35 CA242447-01A1 to V.M.W. This work used: the UCLA Metabolomics Center, supported by NIH Instrumentation Grant S10 OD016387; the Parnassus Flow Cytometry CoLab (PFCC, RRID:*SCR_018206*), supported in part by the DRC Center Grant NIH P30 DK063720.

Author contributions

V.M.W. supervised the project. G.A.T. conceptualized the project. G.A.T., K.M.T., J.t.H., J.F., J.D-A., R.E.V., and V.M.W. procured funding and resources. G.A.T., K.M.T., J.t.H., C.K., J.D-A., and R.E.V. designed experimental methodology. G.A.T., J.t.H., I.B., C.K., J.D-A., and R.E.V. performed experiments and analyzed data. G.A.T. curated data, wrote the manuscript, and edited the manuscript with input from all co-authors.

Data & material availability

All raw data is available upon request & will be made available upon publication of the peer-reviewed manuscript.

Declaration of interests

The authors declare no competing interests.

Figure 1

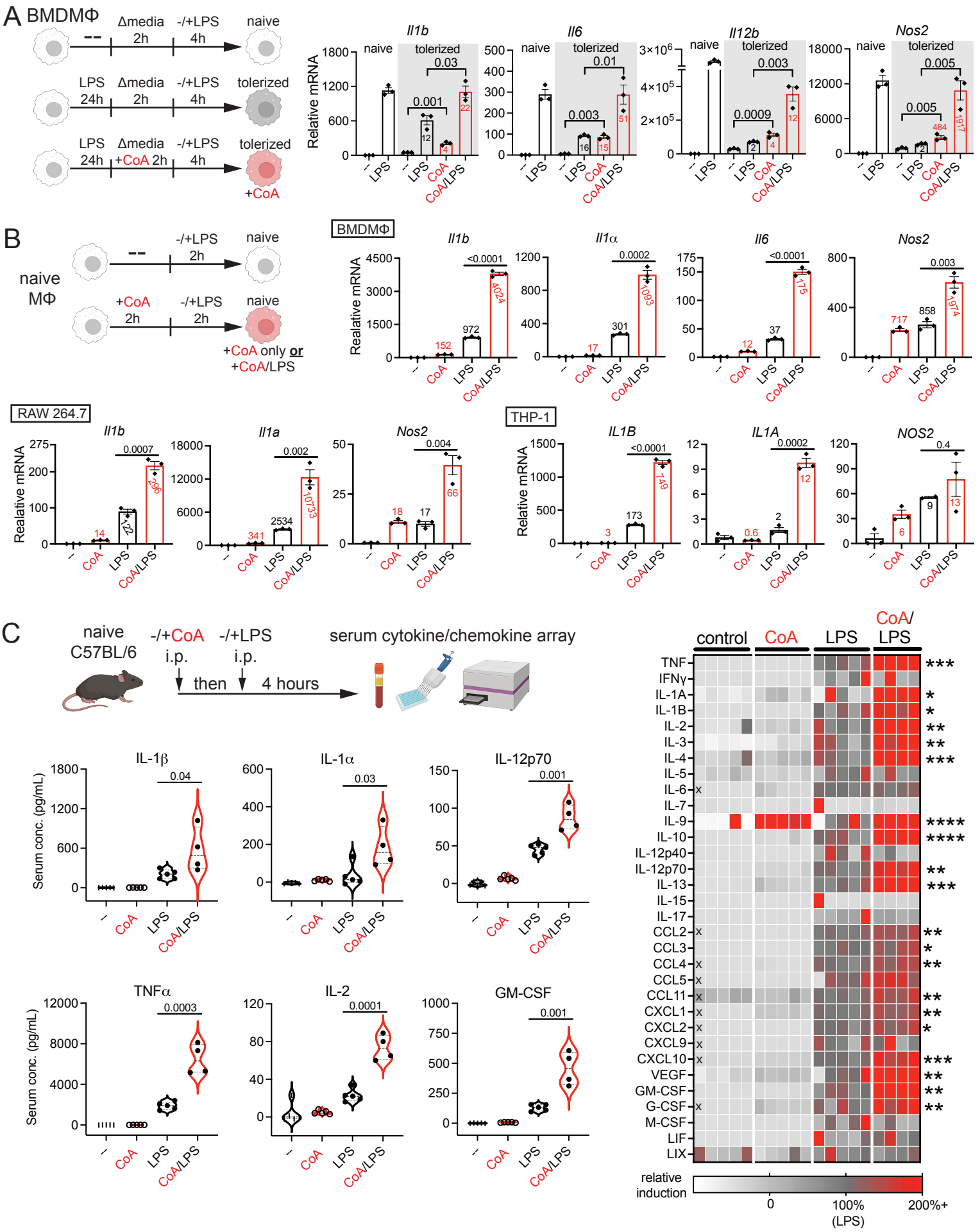
A BMDMΦ
Δmedia 2h
-/+LPS 4h
naive
LPS 24h
tolerized
+CoA 2h
+CoA
Il1b
Il6
Il12b
Nos2
Relative mRNA
B
naive MΦ
+CoA only or +CoA/LPS
BMDMΦ
Il1α
RAW 264.7
Il1a
THP-1
IL1B
IL1A
NOS2
C
naive C57BL/6
-/+CoA i.p.
-/+LPS i.p.
then 4 hours
serum cytokine/chemokine array
IL-1β
IL-1α
IL-12p70
TNFα
IL-2
GM-CSF
Serum conc. (pg/mL)
control
CoA
LPS
CoA/LPS
TNF
IFNγ
IL-1A
IL-1B
IL-2
IL-3
IL-4
IL-5
IL-6
IL-7
IL-9
IL-10
IL-12p40
IL-12p70
IL-13
IL-15
IL-17
CCL2
CCL3
CCL4
CCL5
CCL11
CXCL1
CXCL2
CXCL9
CXCL10
VEGF
GM-CSF
G-CSF
M-CSF
LIF
LIX
relative induction
0
100% (LPS)
200%+

Figure 1. CoA reverses tolerance and enhances TLR-dependent proinflammatory responses *in vitro* and *in vivo*

A. Quantitative realtime PCR (qPCR) for LPS-induced proinflammatory gene expression in naïve or tolerized bone morrow-derived macrophages (BMDMs) with CoA supplementation (2.5mM). Numbers denote fold-induction over the tolerized, untreated condition.

B. qPCR for LPS-induced proinflammatory gene expression in naïve BMDMs, RAW 264.7s, and THP-1s with CoA supplementation (250μM). Numbers denote fold-induction over the untreated condition.

C. Serum levels of select proteins in male C57BL/6 mice intraperitoneally (i.p.) injected with CoA (250 mg/kg), LPS (3 mg/kg), or CoA/LPS. Violin plots for select serum proteins (left), and heatmap showing relative induction of all cytokines, chemokines, and growth factors quantified (right), with induction in "LPS" group set to 100%. For violin plots, numbers above bars are P values from Student's t-test for the indicated conditions (planned comparisons). For heatmap, *P<0.05. *P<0.01, ***P<0.001, and ****P<0.0001 between "LPS" and "CoA/LPS" groups in each row (Student's t-test, planned comparisons). "x" denotes protein for which at least one sample in the "CoA/LPS" group exceeded the linear range of the standard curve, underestimating induction in this group. n=5 mice per group except "CoA/LPS", n=4.

For qPCRs in **A** and **B**, n=3 biological replicates per condition, and numbers above bars are P values from Student's t-test (planned comparisons).

Figure S1

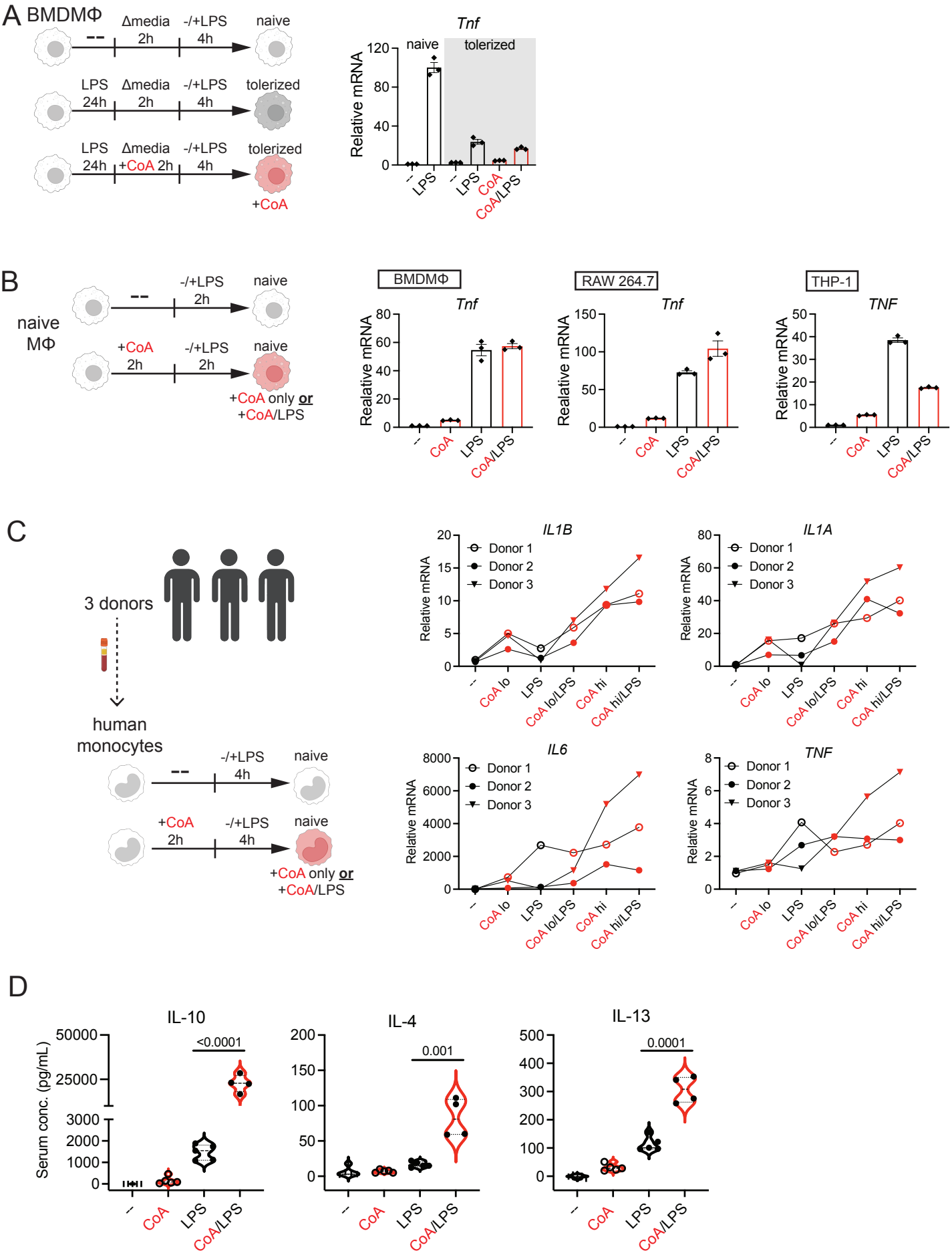
A
BMDMΦ
Δmedia 2h
-/+LPS 4h
naive
LPS 24h
tolerized
+CoA 2h
+CoA
Tnf
naive
tolerized
Relative mRNA
B
naive MΦ
-/+LPS 2h
+CoA 2h
+CoA only or +CoA/LPS
BMDMΦ
RAW 264.7
THP-1
TNF
CoA
LPS
CoA/LPS
C
3 donors
human monocytes
IL1B
IL1A
IL6
TNF
Donor 1
Donor 2
Donor 3
CoA lo
CoA hi
CoA lo/LPS
CoA hi/LPS
D
IL-10
IL-4
IL-13
Serum conc. (pg/mL)
<0.0001
0.001
0.0001

Figure S1.

A. qPCR for LPS-induced *Tnf* expression in naïve or tolerized BMDMs with CoA supplementation (2.5mM)

B. qPCR for LPS-induced *Tnf*/*TNF* expression in naïve BMDMs, RAW 264.7s, and THP-1s with CoA supplementation (250μM). For qPCRs in **A** and **B**, n=3 biological replicates per condition**.**

C. qPCR for proinflammatory gene expression in primary human monocytes from 3 independent donors with CoA supplementation at two doses (lo = 500μM CoA, hi = 5mM CoA) either alone or with LPS.

D. Serum levels of select proteins in male C57BL/6 mice i.p. injected with CoA (250 mg/kg), LPS (3 mg/kg), or CoA/LPS. Numbers above bars are P values from Student's t-test (planned comparisons). n=5 mice per group except "CoA/LPS", n=4.

Figure 2

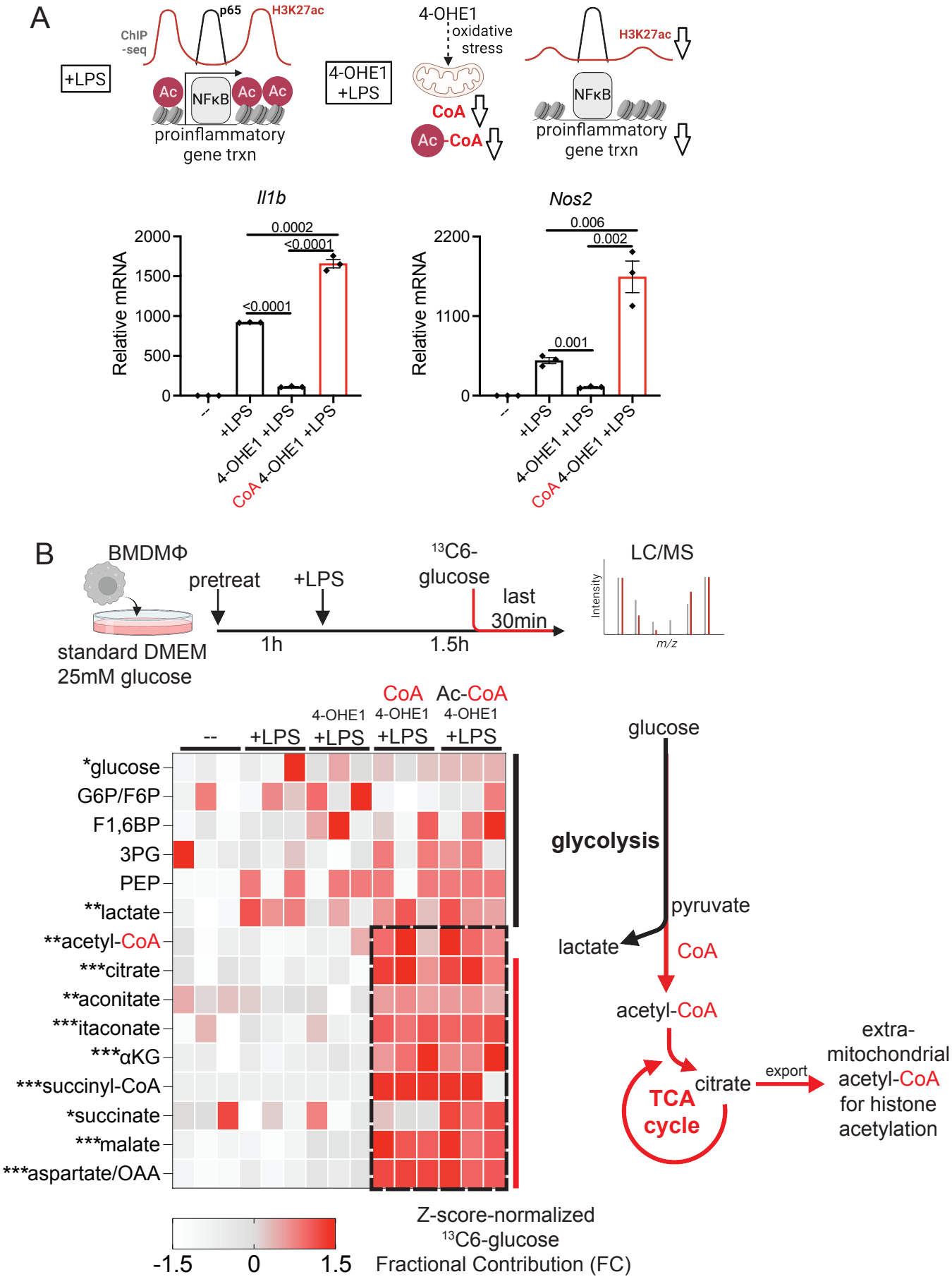
A
ChIP -seq
p65
H3K27ac
+LPS
Ac
NFκB
proinflammatory gene trxn
4-OHE1 +LPS
4-OHE1
oxidative stress
CoA
Ac-CoA
Il1b
Nos2
Relative mRNA
0.0002
<0.0001
0.006
0.002
0.001
--
+LPS
4-OHE1 +LPS
CoA 4-OHE1 +LPS
B
BMDMΦ
standard DMEM
25mM glucose
pretreat
+LPS
13C6-glucose
last 30min
1h
1.5h
LC/MS
Intensity
m/z
CoA
Ac-CoA
4-OHE1
*glucose
G6P/F6P
F1,6BP
3PG
PEP
**lactate
**acetyl-CoA
***citrate
**aconitate
***itaconate
***αKG
***succinyl-CoA
*succinate
***malate
***aspartate/OAA
glucose
glycolysis
pyruvate
lactate
CoA
acetyl-CoA
citrate
TCA cycle
export
extra-mitochondrial acetyl-CoA for histone acetylation
-1.5
0
1.5
Z-score-normalized 13C6-glucose Fractional Contribution (FC)

Figure 2. CoA enhances glucose entry into the mitochondrial TCA cycle.

A. Top – Illustrated summary of 4-OHE1's disruption of CoA and acetyl-CoA homeostasis and LPS-induced histone acetylation. Bottom - qPCR for LPS-induced *Il1b* and *Nos2* in BMDMs (1.5h LPS stimulation) pretreated for 1h with 4-hydroxyestrone (5μM) and/or CoA (250μM) as outlined in **B**. n=3 biological replicates per condition, and numbers above bars are P values from Student's t-test (planned comparisons).

B. Top – experimental design for ^{13}C6-glucose isotope tracing in BMDMs. Competitive labeling of metabolites with ^{13}C6-glucose is performed from the final 30 minutes of a 1.5h LPS stimulation to determine how CoA supplementation influences glucose labeling of metabolites, serving as a proxy for metabolic pathway activity. Bottom – Heatmap depicting ^{13}C6-glucose Fractional Contribution (FC) to glycolytic and TCA cycle metabolites, represented as a Z-score for each metabolite. Metabolites with significant FC differences between conditions were identified by One-Way ANOVA. *P<0.05. *P<0.01,***P<0.001. n=3 biological replicates per condition.

Figure S2

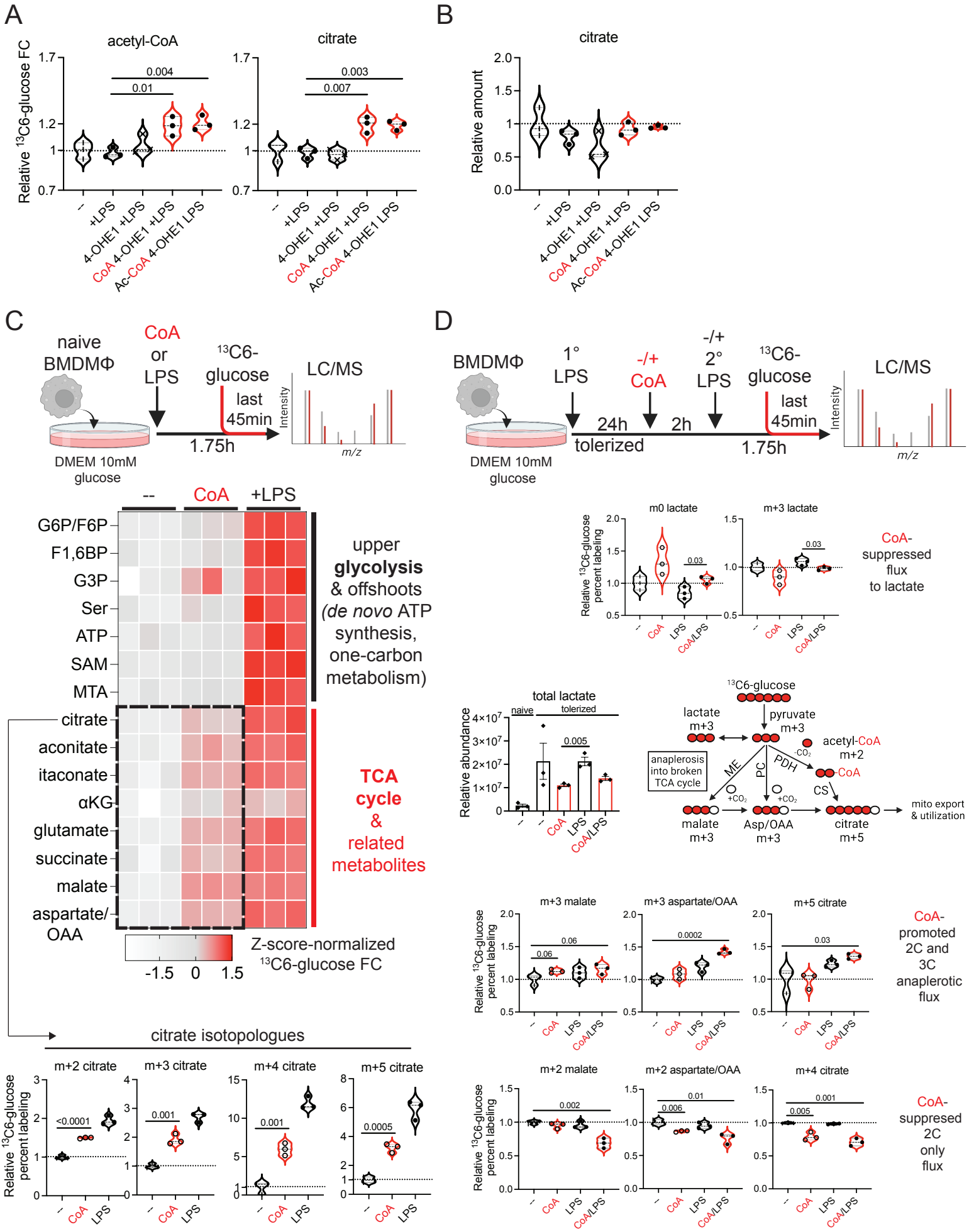
A
acetyl-CoA
citrate
Relative ^{13}C6-glucose FC
0.004
0.01
0.003
0.007
--
+LPS
4-OHE1 +LPS
CoA 4-OHE1 +LPS
Ac-CoA 4-OHE1 LPS
B
citrate
Relative amount
C
naive BMDMΦ
CoA or LPS
^{13}C6-glucose last 45min
LC/MS
Intensity
m/z
DMEM 10mM glucose
1.75h
--
CoA
+LPS
G6P/F6P
F1,6BP
G3P
Ser
ATP
SAM
MTA
citrate
aconitate
itaconate
αKG
glutamate
succinate
malate
aspartate/ OAA
upper glycolysis & offshoots (de novo ATP synthesis, one-carbon metabolism)
TCA cycle & related metabolites
Z-score-normalized ^{13}C6-glucose FC
-1.5
0
1.5
citrate isotopologues
m+2 citrate
m+3 citrate
m+4 citrate
m+5 citrate
Relative ^{13}C6-glucose percent labeling
<0.0001
0.001
0.001
0.0005
D
BMDMΦ
1° LPS
-/+ CoA
-/+ 2° LPS
^{13}C6-glucose last 45min
LC/MS
24h tolerized
2h
1.75h
DMEM 10mM glucose
m0 lactate
m+3 lactate
0.03
0.03
CoA-suppressed flux to lactate
total lactate
naive
tolerized
Relative abundance
0.005
^{13}C6-glucose
lactate m+3
pyruvate m+3
acetyl-CoA m+2
anaplerosis into broken TCA cycle
ME
PC
PDH
CS
malate m+3
Asp/OAA m+3
citrate m+5
mito export & utilization
m+3 malate
m+3 aspartate/OAA
m+5 citrate
0.06
0.06
0.0002
0.03
CoA-promoted 2C and 3C anaplerotic flux
m+2 malate
m+2 aspartate/OAA
m+4 citrate
0.002
0.01
0.006
0.001
0.005
CoA-suppresed 2C only flux

Figure S2.

A. Relative ^{13}C6-glucose FC to acetyl-CoA and citrate from **Fig. 2B** experiment. Numbers above bars are P values from Dunnett's post-hoc test correcting for multiple comparisons.

B. Relative total amount of citrate from experiment in **Fig. 2B**.

C. Top – Heatmap depicting Z-score-normalized ^{13}C6-glucose FC to indicated metabolites in naïve BMDMs treated with CoA (250μM) or LPS for 1.75h. Bottom - Relative ^{13}C6-glucose percent labeling of citrate isotopologues. Numbers above bars are P values from Student's t-test (planned comparisons).

D. Relative ^{13}C6-glucose percent labeling of specific isotopologues of malate, aspartate (a proxy for oxaloacetate), citrate, and lactate, in LPS-tolerized BMDMs treated with CoA (2.5mM), LPS, or CoA/LPS as indicated. Total lactate levels are also shown for naïve versus tolerized macrophages treated as indicated. n=3 biological replicates per condition for all metabolomics experiments. Numbers above bars are P values from Student's t-test (planned comparisons).

Figure 3

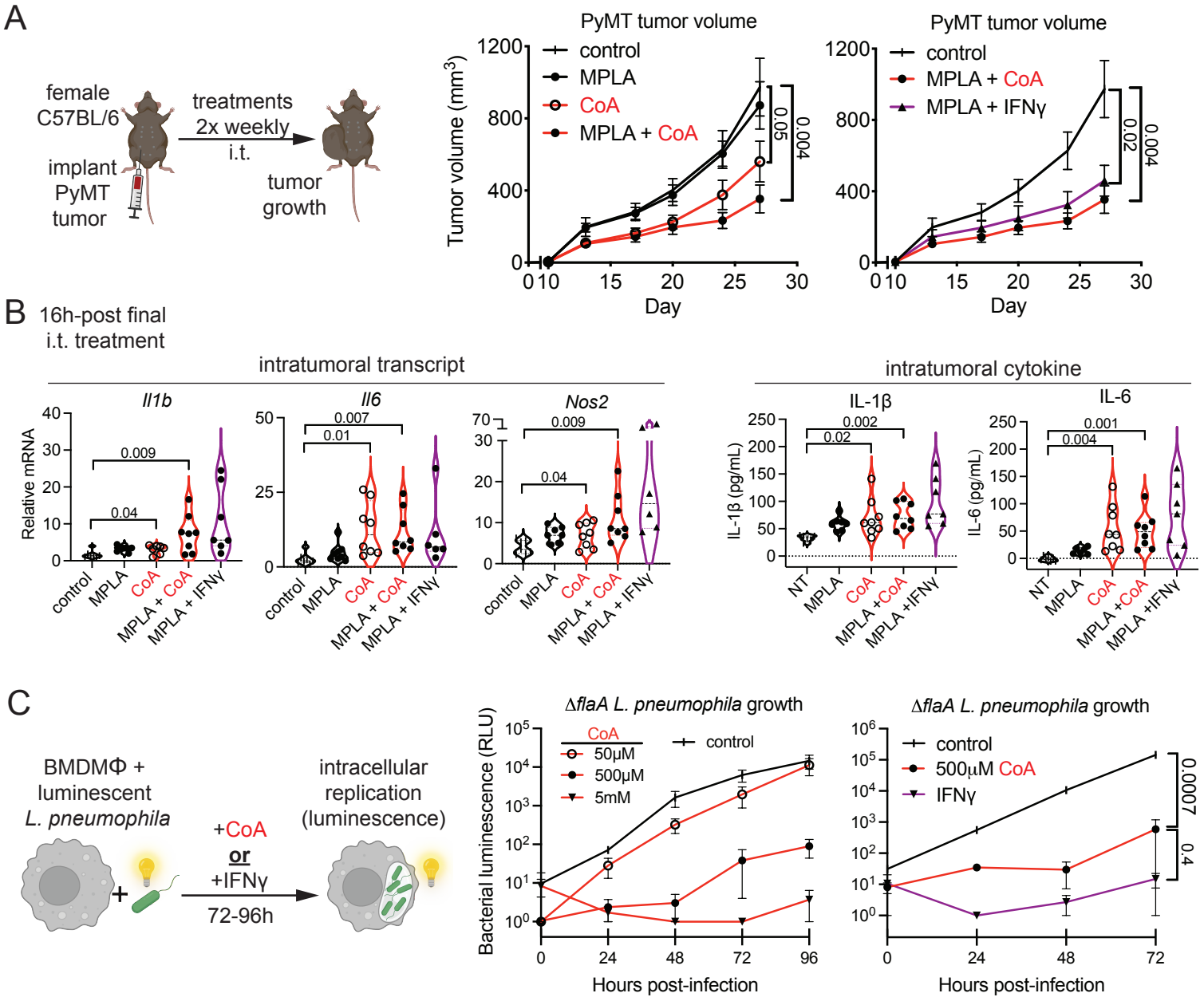
A
female C57BL/6
implant PyMT tumor
treatments 2x weekly i.t.
tumor growth
PyMT tumor volume
Tumor volume (mm3)
control
MPLA
CoA
MPLA + CoA
MPLA + IFNγ
Day
0.05
0.004
0.02
B
16h-post final i.t. treatment
intratumoral transcript
intratumoral cytokine
Il1b
Il6
Nos2
Relative mRNA
IL-1β
IL-6
IL-1β (pg/mL)
IL-6 (pg/mL)
NT
C
BMDMΦ + luminescent L. pneumophila
+CoA or +IFNγ
72-96h
intracellular replication (luminescence)
ΔflaA L. pneumophila growth
Bacterial luminescence (RLU)
Hours post-infection
50μM
500μM
5mM
0.0007
0.4

Figure 3. CoA enhances macrophage-dependent TLR agonist anti-tumor activity and macrophage anti-microbial activity.

A. Orthotopic MMTV-PyMT breast tumor volume in female C57BL/6 mice. Left – volume in control tumors versus tumors treated intratumorally (i.t.) with MPLA, CoA, or MPLA+CoA. Right – volume in control, MPLA+CoA-treated, and MPLA+IFNγ-treated tumors. Numbers represent P values from Student's t-test at Day 27 (planned comparisons). n=8 mice per group.

B. Intratumoral gene expression (left) and cytokine levels (right) from mice in **A**. 16 hours after final i.t. treatment. n=7 or 8 mice per group. Numbers represent P values from Student's t-test (planned comparisons).

C. Luminescent Δ*flaA Legionella pneumophila* intracellular growth in infected BMDMs. Left – intracellular bacterial replication over time in control or CoA-treated BMDMs. Right - intracellular bacterial replication over time in BMDMs treated with CoA or IFNγ. Numbers represent P values from Student's t-test (planned comparisons). n=3 biological replicates per condition.

Figure S3

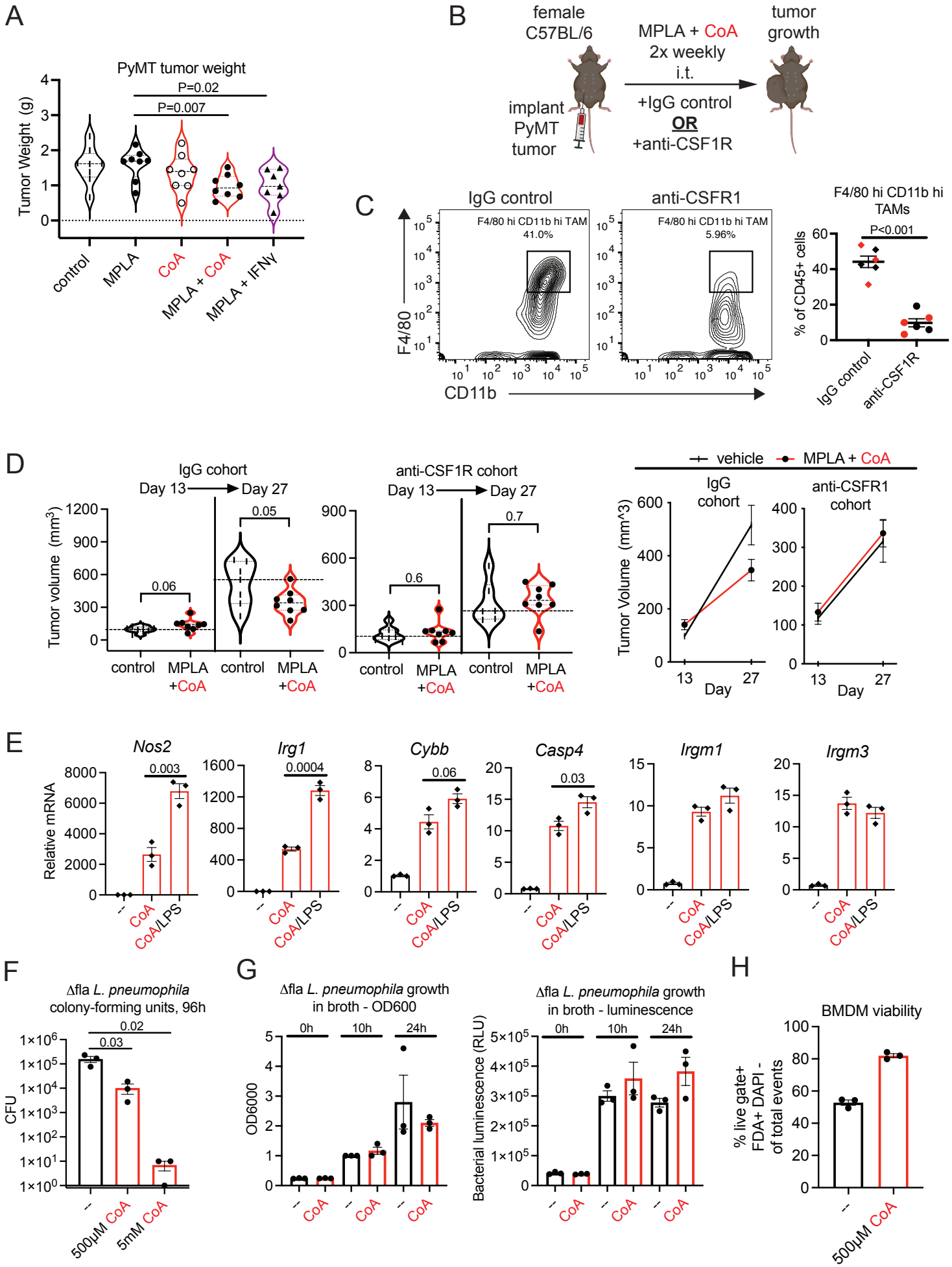
A
PyMT tumor weight
P=0.02
P=0.007
Tumor Weight (g)
control
MPLA
CoA
MPLA + CoA
MPLA + IFNγ
B
female C57BL/6
implant PyMT tumor
MPLA + CoA
2x weekly
i.t.
+IgG control
OR
+anti-CSF1R
tumor growth
C
IgG control
anti-CSFR1
F4/80 hi CD11b hi TAM
41.0%
5.96%
F4/80
CD11b
F4/80 hi CD11b hi TAMs
P<0.001
% of CD45+ cells
IgG control
anti-CSF1R
D
IgG cohort
Day 13
Day 27
anti-CSF1R cohort
Tumor volume (mm3)
0.06
0.05
0.6
0.7
control
MPLA +CoA
vehicle
MPLA + CoA
IgG cohort
anti-CSFR1 cohort
Tumor Volume (mm^3)
Day
E
Nos2
Irg1
Cybb
Casp4
Irgm1
Irgm3
Relative mRNA
0.003
0.0004
0.06
0.03
–
CoA
CoA/LPS
F
Δfla L. pneumophila
colony-forming units, 96h
CFU
0.02
0.03
500μM CoA
5mM CoA
G
Δfla L. pneumophila growth
in broth - OD600
OD6000
0h
10h
24h
Δfla L. pneumophila growth
in broth - luminescence
Bacterial luminescence (RLU)
H
BMDM viability
% live gate+ FDA+ DAPI - of total events
500μM CoA

Figure S3.

A. Day 30 tumor weights from mice in **Fig. 3A**.

B. Experimental strategy to test the contribution of tumor-associated macrophages (TAMs) to the anti-tumor effect of MPLA+CoA therapy.

C. Left – flow cytometry of CD45+ tumor cells depicting F4/80 hi CD11b hi TAM populations in representative mice from IgG control antibody-treated or anti-CSF1R antibody-treated cohorts. Right – quantification of flow cytometry results confirming TAM depletion in anti-CSF1R-treated mice. 6 mice were chosen at random from the IgG control or anti-CSF1R cohorts. Black indicates mice receiving vehicle control treatment, red indicates mice receiving MPLA+CoA therapy.

D. Effects of TAM depletion on MPLA+CoA therapy efficacy, represented by comparing tumor size among all animals (left), or by comparing tumor growth rates (right), on experimental Days 13 and 27 between IgG and anti-CSFR1 cohorts receiving vehicle or MPLA+CoA therapy. n=8 or 7 mice per group.

E. qPCR for *L. pneumophila* restriction genes in BMDMs treated with CoA alone (500μM), or CoA in combination with LPS. Numbers represent P values from Student's t-test (planned comparisons). n=3 biological replicates per condition.

F. *L. pneumophila* colony forming units (CFUs) from infected BMDMs in **Fig. 3C**, left, 96h after infection.

G. *L. pneumophila* growth (left) and luminescence (right) in broth supplemented with 500μM CoA for 24 hours. n=3 biological replicates per condition.

H. BMDM viability assessed by flow cytometry after 72h of continuous 500μM CoA supplementation. n=3 biological replicates per condition.

Figure 4

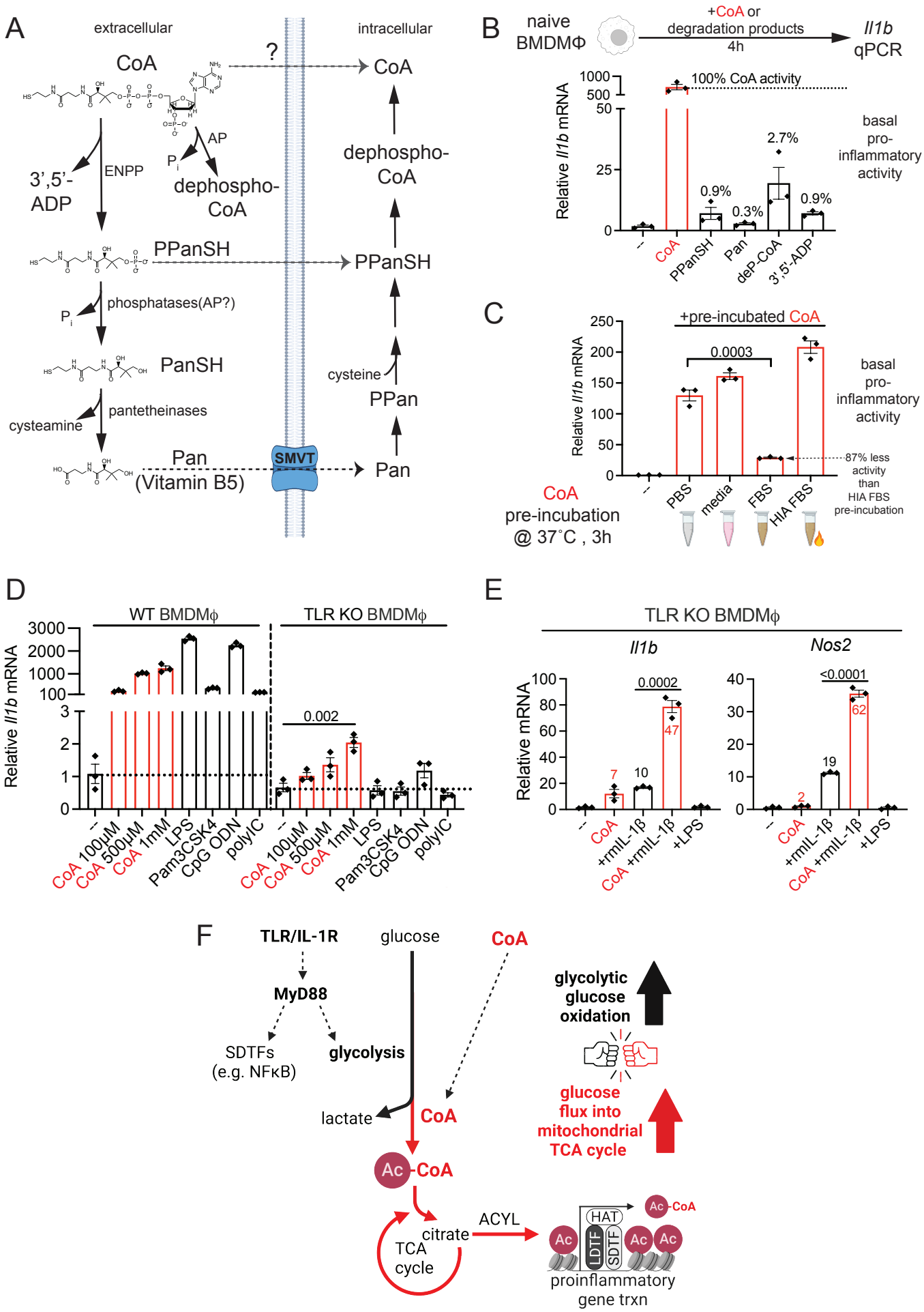
A
extracellular
intracellular
CoA
?
CoA
AP
ENPP
3',5'-ADP
dephospho-CoA
dephospho-CoA
PPanSH
PPanSH
phosphatases(AP?)
PanSH
cysteine
PPan
pantetheinases
cysteamine
Pan
(Vitamin B5)
SMVT
Pan
B
naive BMDMΦ
+CoA or degradation products
4h
Il1b qPCR
Relative Il1b mRNA
100% CoA activity
basal pro-inflammatory activity
0.9%
0.3%
2.7%
0.9%
--
CoA
PPanSH
Pan
deP-CoA
3',5'-ADP
C
+pre-incubated CoA
Relative Il1b mRNA
0.0003
basal pro-inflammatory activity
87% less activity than HIA FBS pre-incubation
CoA pre-incubation @ 37˚C , 3h
PBS
media
FBS
HIA FBS
D
WT BMDMϕ
TLR KO BMDMϕ
Relative Il1b mRNA
0.002
CoA 100μM
CoA 500μM
CoA 1mM
LPS
Pam3CSK4
CpG ODN
polyIC
E
TLR KO BMDMϕ
Il1b
Nos2
Relative mRNA
0.0002
<0.0001
+rmIL-1β
CoA +rmIL-1β
+LPS
F
TLR/IL-1R
glucose
CoA
MyD88
SDTFs (e.g. NFκB)
glycolysis
lactate
CoA
Ac-CoA
citrate
TCA cycle
ACYL
HAT
LDTF
SDTF
Ac
proinflammatory gene trxn
glycolytic glucose oxidation
glucose flux into mitochondrial TCA cycle

Figure 4. CoA's enhancement of proinflammatory gene transcription requires direct CoA uptake and TLR signaling.

A. Schematic depicting known pathways of extracellular CoA degradation product entry into intracellular CoA biosynthesis pathway.

B. *Il1b* qPCR in BMDMs treated with CoA or CoA degradation products (500μM). Percentages represent *Il1b* induction relative to CoA.

C. *Il1b* qPCR in BMDMs treated with CoA (500μM) for 2h. Prior to addition to BMDMs ,CoA was preincubated at 37°C for 3h in PBS, media, non-heat inactivated FBS, of heat-inactivated (HIA) FBS.

D. *Il1b* qPCR in WT and TLR KO BMDMs treated with CoA or TLR ligands for 4h.

E. *Il1b* qPCR in WT and TLR KO BMDMs pretreated with 500μM CoA for 2h before stimulation with 50 ng/mL recombinant mouse IL-1β for 4h.

F. Model depicting how CoA routes glucose into the mitochondrial TCA cycle, cooperating with TLR signaling to provide requisite metabolic-epigenetic support of proinflammatory gene transcription.

n=3 biological replicates per condition for all qPCRs, and numbers above bars are P values from Student's t-test (planned comparisons).

Figure S4

A

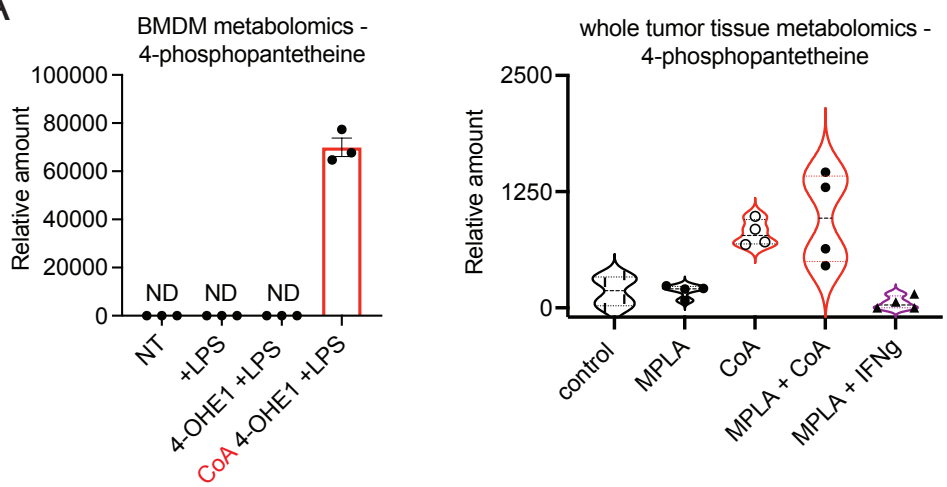

B

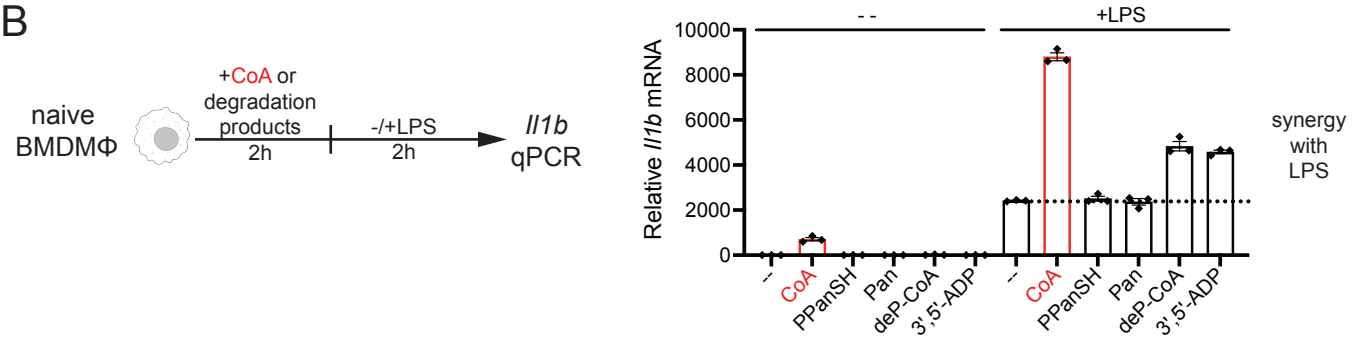

C

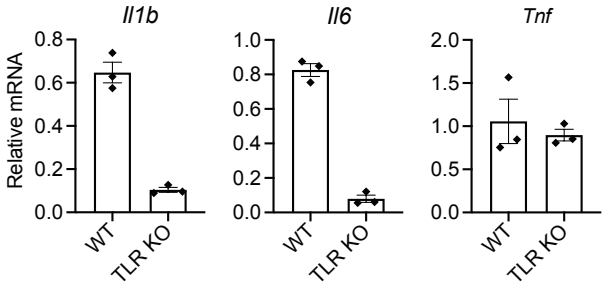

Figure S4.

A. 4-phosphopantetheine (PPanSH) levels in BMDMs supplemented with CoA (left), or in tumors receiving i.t. CoA from **Fig. 3A** (right) as quantified from polar metabolite cell/tissue extracts. ND = not detected.

B. *Il1b* qPCR in BMDMs treated with CoA or CoA degradation products alone (500μM, left), or in combination with LPS (right).

C. qPCR measuring basal expression of proinflammatory genes in WT versus TLR KO BMDMs in the absence of exogenously added TLR ligands.

n=3 or 4 biological replicates per condition for all metabolomics and qPCR data.

References

1. Q. Zhang, M. Raoof, Y. Chen, Y. Sumi, T. Sursal, W. Junger, K. Brohi, K. Itagaki, C. J. Hauser, Circulating Mitochondrial DAMPs Cause Inflammatory Responses to Injury. *Nature*. **464**, 104–107 (2010).
2. M. Divangahi, P. Aaby, S. A. Khader, L. B. Barreiro, S. Bekkering, T. Chavakis, R. van Crevel, N. Curtis, A. R. DiNardo, J. Dominguez-Andres, R. Duivenvoorden, S. Fanucchi, Z. Fayad, E. Fuchs, M. Hamon, K. L. Jeffrey, N. Khan, L. A. B. Joosten, E. Kaufmann, E. Latz, G. Matarese, J. W. M. van der Meer, M. Mhlanga, S. J. C. F. M. Moorlag, W. J. M. Mulder, S. Naik, B. Novakovic, L. O'Neill, J. Ochando, K. Ozato, N. P. Riksen, R. Sauerwein, E. R. Sherwood, A. Schlitzer, J. L. Schultze, M. H. Sieweke, C. S. Benn, H. Stunnenberg, J. Sun, F. L. van de Veerdonk, S. Weis, D. L. Williams, R. Xavier, M. G. Netea, Trained immunity, tolerance, priming and differentiation: distinct immunological processes. *Nat Immunol*. **22**, 2–6 (2021).
3. O. M. Pena, J. Pistolic, D. Raj, C. D. Fjell, R. E. Hancock, Endotoxin tolerance represents a distinctive state of alternative polarization (M2) in human mononuclear cells. *Journal of immunology (Baltimore, Md.: 1950)*. **186**, 7243–7254 (2011).
4. C. Porta, M. Rimoldi, G. Raes, L. Brys, P. Ghezzi, D. D. Liberto, F. Dieli, S. Ghisletti, G. Natoli, P. D. Baetselier, A. Mantovani, A. Sica, Tolerance and M2 (alternative) macrophage polarization are related processes orchestrated by p50 nuclear factor kappaB. *Proceedings of the National Academy of Sciences of the United States of America*. **106**, 14978–14983 (2009).
5. L. M. Sly, M. J. Rauh, J. Kalesnikoff, C. H. Song, G. Krystal, LPS-induced upregulation of SHIP is essential for endotoxin tolerance. *Immunity*. **21**, 227–239 (2004).
6. D. Zhang, Z. Tang, H. Huang, G. Zhou, C. Cui, Y. Weng, W. Liu, S. Kim, S. Lee, M. Perez-Neut, J. Ding, D. Czyz, R. Hu, Z. Ye, M. He, Y. G. Zheng, H. A. Shuman, L. Dai, B. Ren, R. G. Roeder, L. Becker, Y. Zhao, Metabolic regulation of gene expression by histone lactylation. *Nature*. **574**, 575–580 (2019).
7. R. A. Irizarry-Caro, M. M. McDaniel, G. R. Overcast, V. G. Jain, T. D. Troutman, C. Pasare, TLR signaling adapter BCAP regulates inflammatory to reparatory macrophage transition by promoting histone lactylation. *Proc Natl Acad Sci U S A*. **117**, 30628–30638 (2020).
8. M. Nguyen-Chi, B. Laplace-Builhe, J. Travnickova, P. Luz-Crawford, G. Tejedor, Q. T. Phan, I. Duroux-Richard, J. P. Levraud, K. Kissa, G. Lutfalla, C. Jorgensen, F. Djouad, Identification of polarized macrophage subsets in zebrafish. *eLife*. **4**, e07288 (2015).
9. R. S. Hotchkiss, G. Monneret, D. Payen, Sepsis-induced immunosuppression: from cellular dysfunctions to immunotherapy. *Nature reviews.Immunology*. **13**, 862–874 (2013).
10. F. Venet, G. Monneret, Advances in the understanding and treatment of sepsis-induced immunosuppression. *Nat Rev Nephrol*. **14**, 121–137 (2018).
11. M. L. Washburn, Z. Wang, A. H. Walton, S. P. Goedegebuure, D. J. Figueroa, S. V. Horn, J. Grossman, K. Remlinger, H. Madsen, J. Brown, R. Srinivasan, A. I. Wolf, S. B. Berger, V. N. Yi, W. G. Hawkins, R. C. Fields, R. S. Hotchkiss, T Cell- and Monocyte-Specific RNA-

Sequencing Analysis in Septic and Nonseptic Critically Ill Patients and in Patients with Cancer. *Journal of immunology (Baltimore, Md.: 1950)*. **203**, 1897–1908 (2019).
12. L. Sun, T. Kees, A. S. Almeida, B. Liu, X. Y. He, D. Ng, X. Han, D. L. Spector, I. A. McNeish, P. Gimotty, S. Adams, M. Egeblad, Activating a collaborative innate-adaptive immune response to control metastasis. *Cancer cell*. **39**, 1361-1374.e9 (2021).
13. S.-C. Cheng, B. P. Scicluna, R. J. W. Arts, M. S. Gresnigt, E. Lachmandas, E. J. Giamarellos-Bourboulis, M. Kox, G. R. Manjeri, J. A. L. Wagenaars, O. L. Cremer, J. Leentjens, A. J. van der Meer, F. L. van de Veerdonk, M. J. Bonten, M. J. Schultz, P. H. G. M. Willems, P. Pickkers, L. A. B. Joosten, T. van der Poll, M. G. Netea, Broad defects in the energy metabolism of leukocytes underlie immunoparalysis in sepsis. *Nat Immunol*. **17**, 406–413 (2016).
14. S. Galván-Peña, L. A. O'Neill, Metabolic reprograming in macrophage polarization. *Frontiers in immunology*. **5**, 420 (2014).
15. P. K. Langston, A. Nambu, J. Jung, M. Shibata, H. I. Aksoylar, J. Lei, P. Xu, M. T. Doan, H. Jiang, M. R. MacArthur, X. Gao, Y. Kong, E. T. Chouchani, J. W. Locasale, N. W. Snyder, T. Horng, Glycerol phosphate shuttle enzyme GPD2 regulates macrophage inflammatory responses. *Nature immunology*. **20**, 1186–1195 (2019).
16. M. A. Lauterbach, J. E. Hanke, M. Serefidou, M. S. J. Mangan, C. C. Kolbe, T. Hess, M. Rothe, R. Kaiser, F. Hoss, J. Gehlen, G. Engels, M. Kreutzenbeck, S. V. Schmidt, A. Christ, A. Imhof, K. Hiller, E. Latz, Toll-like Receptor Signaling Rewires Macrophage Metabolism and Promotes Histone Acetylation via ATP-Citrate Lyase. *Immunity*. **51**, 997-1011.e7 (2019).
17. G. A. Timblin, K. M. Tharp, B. Ford, J. M. Winchester, J. Wang, S. Zhu, R. I. Khan, S. K. Louie, A. T. Iavarone, J. T. Hoeve, D. K. Nomura, A. Stahl, K. Saijo, Mitohormesis reprogrammes macrophage metabolism to enforce tolerance. *Nature metabolism*. **3**, 618–635 (2021).
18. O. R. Colegio, N.-Q. Chu, A. L. Szabo, T. Chu, A. M. Rhebergen, V. Jairam, N. Cyrus, C. E. Brokowski, S. C. Eisenbarth, G. M. Phillips, G. W. Cline, A. J. Phillips, R. Medzhitov, Functional polarization of tumour-associated macrophages by tumour-derived lactic acid. *Nature*. **513**, 559–563 (2014).
19. I. Gout, Coenzyme A, protein CoAlation and redox regulation in mammalian cells. *Biochemical Society transactions*. **46**, 721–728 (2018).
20. B. Beutler, E. T. Rietschel, Innate immune sensing and its roots: the story of endotoxin. *Nat Rev Immunol*. **3**, 169–176 (2003).
21. R. N. Moore, K. J. Goodrum, L. J. Berry, Mediation of an endotoxic effect by macrophages. *J Reticuloendothel Soc*. **19**, 187–197 (1976).
22. W. Yu, Z. Wang, K. Zhang, Z. Chi, T. Xu, D. Jiang, S. Chen, W. Li, X. Yang, X. Zhang, Y. Wu, D. Wang, One-Carbon Metabolism Supports S-Adenosylmethionine and Histone Methylation to Drive Inflammatory Macrophages. *Molecular cell*. **75**, 1147-1160.e5 (2019).
23. A. Adina-Zada, T. N. Zeczycki, P. V. Attwood, Regulation of the structure and activity of pyruvate carboxylase by acetyl CoA. *Arch Biochem Biophys*. **519**, 118–130 (2012).

24. E. M. Palmieri, M. Gonzalez-Cotto, W. A. Baseler, L. C. Davies, B. Ghesquière, N. Maio, C. M. Rice, T. A. Rouault, T. Cassel, R. M. Higashi, A. N. Lane, T. W.-M. Fan, D. A. Wink, D. W. McVicar, Nitric oxide orchestrates metabolic rewiring in M1 macrophages by targeting aconitase 2 and pyruvate dehydrogenase. *Nat Commun*. **11**, 698 (2020).
25. V. Lampropoulou, A. Sergushichev, M. Bambouskova, S. Nair, E. E. Vincent, E. Loginicheva, L. Cervantes-Barragan, X. Ma, S. C. Huang, T. Griss, C. J. Weinheimer, S. Khader, G. J. Randolph, E. J. Pearce, R. G. Jones, A. Diwan, M. S. Diamond, M. N. Artyomov, Itaconate Links Inhibition of Succinate Dehydrogenase with Macrophage Metabolic Remodeling and Regulation of Inflammation. *Cell metabolism*. **24**, 158–166 (2016).
26. G. L. Seim, E. C. Britt, S. V. John, F. J. Yeo, A. R. Johnson, R. S. Eisenstein, D. J. Pagliarini, J. Fan, Two-stage metabolic remodelling in macrophages in response to lipopolysaccharide and interferon-γ stimulation. *Nature metabolism*. **1**, 731–742 (2019).
27. D. Aminin, Y.-M. Wang, Macrophages as a "weapon" in anticancer cellular immunotherapy. *Kaohsiung J Med Sci*. **37**, 749–758 (2021).
28. X. Chen, Y. Zhang, Y. Fu, The critical role of Toll-like receptor-mediated signaling in cancer immunotherapy. *Medicine in Drug Discovery*. **14**, 100122 (2022).
29. A. Mantovani, A. Sica, Macrophages, innate immunity and cancer: balance, tolerance, and diversity. *Curr Opin Immunol*. **22**, 231–237 (2010).
30. E. López-Collazo, C. del Fresno, Pathophysiology of endotoxin tolerance: mechanisms and clinical consequences. *Crit Care*. **17**, 242 (2013).
31. K. Zubair, C. You, G. Kwon, K. Kang, Two Faces of Macrophages: Training and Tolerance. *Biomedicines*. **9**, 1596 (2021).
32. C. Hernandez, P. Huebener, R. F. Schwabe, Damage-associated molecular patterns in cancer: a double-edged sword. *Oncogene*. **35**, 5931–5941 (2016).
33. O. Maller, A. P. Drain, A. S. Barrett, S. Borgquist, B. Ruffell, I. Zakharevich, T. T. Pham, T. Gruosso, H. Kuasne, J. N. Lakins, I. Acerbi, J. M. Barnes, T. Nemkov, A. Chauhan, J. Gruenberg, A. Nasir, O. Bjarnadottir, Z. Werb, P. Kabos, Y.-Y. Chen, E. S. Hwang, M. Park, L. M. Coussens, A. C. Nelson, K. C. Hansen, V. M. Weaver, Tumour-associated macrophages drive stromal cell-dependent collagen crosslinking and stiffening to promote breast cancer aggression. *Nat. Mater.* **20**, 548–559 (2021).
34. R. B. Lorsbach, W. J. Murphy, C. J. Lowenstein, S. H. Snyder, S. W. Russell, Expression of the nitric oxide synthase gene in mouse macrophages activated for tumor cell killing. Molecular basis for the synergy between interferon-gamma and lipopolysaccharide. *Journal of Biological Chemistry*. **268**, 1908–1913 (1993).
35. F. Arenzana-Seisdedos, J. L. Virelizier, W. Fiers, Interferons as macrophage-activating factors. III. Preferential effects of interferon-gamma on the interleukin 1 secretory potential of fresh or aged human monocytes. *J Immunol*. **134**, 2444–2448 (1985).
36. A. Mackensen, C. Galanos, R. Engelhardt, Modulating activity of interferon-gamma on endotoxin-induced cytokine production in cancer patients. *Blood*. **78**, 3254–3258 (1991).

37. J. G. Haas, N. Meyer, G. Riethmüller, H. W. Ziegler-Heitbrock, Inhibition of lipopolysaccharide-induced in vitro desensitization by interferon-gamma. *Eur J Immunol*. **20**, 1181–1184 (1990).
38. J. Chen, L. B. Ivashkiv, IFN-γ abrogates endotoxin tolerance by facilitating Toll-like receptor-induced chromatin remodeling. *Proceedings of the National Academy of Sciences of the United States of America*. **107**, 19438–19443 (2010).
39. W. D. Döcke, F. Randow, U. Syrbe, D. Krausch, K. Asadullah, P. Reinke, H. D. Volk, W. Kox, Monocyte deactivation in septic patients: restoration by IFN-gamma treatment. *Nature medicine*. **3**, 678–681 (1997).
40. E. Müller, P. F. Christopoulos, S. Halder, A. Lunde, K. Beraki, M. Speth, I. Øynebråten, A. Corthay, Toll-Like Receptor Ligands and Interferon-γ Synergize for Induction of Antitumor M1 Macrophages. *Front Immunol*. **8**, 1383 (2017).
41. D. Duluc, M. Corvaisier, S. Blanchard, L. Catala, P. Descamps, E. Gamelin, S. Ponsoda, Y. Delneste, M. Hebbar, P. Jeannin, Interferon-gamma reverses the immunosuppressive and protumoral properties and prevents the generation of human tumor-associated macrophages. *Int J Cancer*. **125**, 367–373 (2009).
42. F. Sato-Kaneko, S. Yao, A. Ahmadi, S. S. Zhang, T. Hosoya, M. M. Kaneda, J. A. Varner, M. Pu, K. S. Messer, C. Guiducci, R. L. Coffman, K. Kitaura, T. Matsutani, R. Suzuki, D. A. Carson, T. Hayashi, E. E. Cohen, *JCI insight*, in press, doi:93397 [pii].
43. M.-A. N. Jallad, A. R. Jurjus, E. A. Rahal, A. M. Abdelnoor, Triple Immunotherapy Overcomes Immune Evasion by Tumor in a Melanoma Mouse Model. *Front Oncol*. **10**, 839 (2020).
44. P. Escoll, C. Buchrieser, Metabolic reprogramming of host cells upon bacterial infection: Why shift to a Warburg-like metabolism? *The FEBS Journal*. **285**, 2146–2160 (2018).
45. E. Ramond, A. Jamet, M. Coureuil, A. Charbit, Pivotal Role of Mitochondria in Macrophage Response to Bacterial Pathogens. *Frontiers in Immunology*. **10** (2019) (available at https://www.frontiersin.org/article/10.3389/fimmu.2019.02461).
46. H. Borges da Silva, R. Fonseca, J. M. Alvarez, M. R. D'Império Lima, IFN-γ Priming Effects on the Maintenance of Effector Memory CD4+ T Cells and on Phagocyte Function: Evidences from Infectious Diseases. *J Immunol Res*. **2015**, 202816 (2015).
47. G. Kak, M. Raza, B. K. Tiwari, Interferon-gamma (IFN-γ): Exploring its implications in infectious diseases. *Biomol Concepts*. **9**, 64–79 (2018).
48. M. Palusinska-Szysz, M. Janczarek, Innate immunity to Legionella and toll-like receptors — review. *Folia Microbiol*. **55**, 508–514 (2010).
49. P. Escoll, O. R. Song, F. Viana, B. Steiner, T. Lagache, J. C. Olivo-Marin, F. Impens, P. Brodin, H. Hilbi, C. Buchrieser, Legionella pneumophila Modulates Mitochondrial Dynamics to Trigger Metabolic Repurposing of Infected Macrophages. *Cell host & microbe*. **22**, 302-316.e7 (2017).

50. J. Fu, M. Zhou, M. A. Gritsenko, E. S. Nakayasu, L. Song, Z.-Q. Luo, Legionella pneumophila modulates host energy metabolism by ADP-ribosylation of ADP/ATP translocases. *eLife*. **11**, e73611 (2022).
51. J. Noack, D. Jimenez-Morales, E. Stevenson, T. Moss, G. Jang, N. J. Krogan, D. L. Swaney, S. Mukherjee, *bioRxiv*, in press, doi:10.1101/2020.05.19.105395.
52. J. V. Price, D. Russo, D. X. Ji, R. A. Chavez, L. DiPeso, A. Y. Lee, J. Coers, R. E. Vance, IRG1 and Inducible Nitric Oxide Synthase Act Redundantly with Other Interferon-Gamma-Induced Factors To Restrict Intracellular Replication of Legionella pneumophila. *mBio*. **10**, e02629-19 (2019).
53. A. V. Gonçalves, S. R. Margolis, G. F. S. Quirino, D. P. A. Mascarenhas, I. Rauch, R. D. Nichols, E. Ansaldo, M. F. Fontana, R. E. Vance, D. S. Zamboni, Gasdermin-D and Caspase-7 are the key Caspase-1/8 substrates downstream of the NAIP5/NLRC4 inflammasome required for restriction of Legionella pneumophila. *PLoS Pathog*. **15**, e1007886 (2019).
54. Restriction of Legionella pneumophila growth in macrophages requires the concerted action of cytokine and Naip5/Ipaf signalling pathways - Coers - 2007 - Cellular Microbiology - Wiley Online Library, (available at https://onlinelibrary.wiley.com/doi/10.1111/j.1462-5822.2007.00963.x).
55. B. Srinivasan, M. Baratashvili, M. van der Zwaag, B. Kanon, C. Colombelli, R. A. Lambrechts, O. Schaap, E. A. Nollen, A. Podgorsek, G. Kosec, H. Petkovic, S. Hayflick, V. Tiranti, D. J. Reijngoud, N. A. Grzeschik, O. C. Sibon, Extracellular 4'-phosphopantetheine is a source for intracellular coenzyme A synthesis. *Nature chemical biology*. **11**, 784–792 (2015).
56. P. Naquet, E. W. Kerr, S. D. Vickers, R. Leonardi, Regulation of coenzyme A levels by degradation: the "Ins and Outs." *Prog Lipid Res*. **78**, 101028 (2020).
57. S. Heinz, C. E. Romanoski, C. Benner, C. K. Glass, The selection and function of cell type-specific enhancers. *Nature reviews.Molecular cell biology*. **16**, 144–154 (2015).
58. Y. Tan, J. C. Kagan, Innate Immune Signaling Organelles Display Natural and Programmable Signaling Flexibility. *Cell*. **177**, 384-398.e11 (2019).
59. L. Bosurgi, Y. G. Cao, M. Cabeza-Cabrerizo, A. Tucci, L. D. Hughes, Y. Kong, J. S. Weinstein, P. Licona-Limon, E. T. Schmid, F. Pelorosso, N. Gagliani, J. E. Craft, R. A. Flavell, S. Ghosh, C. V. Rothlin, Macrophage function in tissue repair and remodeling requires IL-4 or IL-13 with apoptotic cells. *Science*. **356**, 1072–1076 (2017).
60. K. E. Sivick, N. Arpaia, G. L. Reiner, B. L. Lee, B. R. Russell, G. M. Barton, Toll-like receptor deficient mice reveal how innate immune signaling influences Salmonella virulence strategies. *Cell Host Microbe*. **15**, 203–213 (2014).
61. L. Cai, B. M. Sutter, B. Li, B. P. Tu, Acetyl-CoA Induces Cell Growth and Proliferation by Promoting the Acetylation of Histones at Growth Genes. *Mol Cell*. **42**, 426–437 (2011).
62. L. Shi, B. P. Tu, Acetyl-CoA induces transcription of the key G1 cyclin CLN3 to promote entry into the cell division cycle in Saccharomyces cerevisiae. *Proc Natl Acad Sci U S A*. **110**, 7318–7323 (2013).

63. J. V. Lee, A. Carrer, S. Shah, N. W. Snyder, S. Wei, S. Venneti, A. J. Worth, Z.-F. Yuan, H.-W. Lim, S. Liu, E. Jackson, N. M. Aiello, N. B. Haas, T. R. Rebbeck, A. Judkins, K.-J. Won, L. A. Chodosh, B. A. Garcia, B. Z. Stanger, M. D. Feldman, I. A. Blair, K. E. Wellen, Akt-dependent metabolic reprogramming regulates tumor cell histone acetylation. *Cell Metab*. **20**, 306–319 (2014).
64. A. A. Cluntun, H. Huang, L. Dai, X. Liu, Y. Zhao, J. W. Locasale, The rate of glycolysis quantitatively mediates specific histone acetylation sites. *Cancer Metab*. **3**, 10 (2015).
65. Y. Wen, J. Gu, S.-L. Li, M. A. Reddy, R. Natarajan, J. L. Nadler, Elevated Glucose and Diabetes Promote Interleukin-12 Cytokine Gene Expression in Mouse Macrophages. *Endocrinology*. **147**, 2518–2525 (2006).
66. K. Honma, C. Machida, K. Mochizuki, T. Goda, Glucose and TNF enhance expression of TNF and IL1B, and histone H3 acetylation and K4/K36 methylation, in juvenile macrophage cells. *Gene X*. **5**, 100034 (2020).
67. K. M. Tharp, K. Kersten, O. M. Maller, G. A. Timblin, C. Stashko, M.-K. Hayward, I. Berestjuk, J. ten Hoeve-Scott, B. Samad, A. J. Combes, V. M. Weaver, Myeloid mechano-metabolic programming restricts anti-tumor immunity (2022), p. 2022.07.14.499764, , doi:10.1101/2022.07.14.499764.
68. B. I. Reinfeld, M. Z. Madden, M. M. Wolf, A. Chytil, J. E. Bader, A. R. Patterson, A. Sugiura, A. S. Cohen, A. Ali, B. T. Do, A. Muir, C. A. Lewis, R. A. Hongo, K. L. Young, R. E. Brown, V. M. Todd, T. Huffstater, A. Abraham, R. T. O'Neil, M. H. Wilson, F. Xin, M. N. Tantawy, W. D. Merryman, R. W. Johnson, C. S. Williams, E. F. Mason, F. M. Mason, K. E. Beckermann, M. G. Vander Heiden, H. C. Manning, J. C. Rathmell, W. K. Rathmell, Cell-programmed nutrient partitioning in the tumour microenvironment. *Nature*. **593**, 282–288 (2021).
69. K. I. Onyedibe, M. Wang, H. O. Sintim, ENPP1, an Old Enzyme with New Functions, and Small Molecule Inhibitors—A STING in the Tale of ENPP1. *Molecules*. **24**, 4192 (2019).
70. In vitro induction of trained immunity in adherent human monocytes: STAR Protocols, (available at https://star-protocols.cell.com/protocols/490).
71. J. M. Buescher, M. R. Antoniewicz, L. G. Boros, S. C. Burgess, H. Brunengraber, C. B. Clish, R. J. DeBerardinis, O. Feron, C. Frezza, B. Ghesquiere, E. Gottlieb, K. Hiller, R. G. Jones, J. J. Kamphorst, R. G. Kibbey, A. C. Kimmelman, J. W. Locasale, S. Y. Lunt, O. D. Maddocks, C. Malloy, C. M. Metallo, E. J. Meuillet, J. Munger, K. Noh, J. D. Rabinowitz, M. Ralser, U. Sauer, G. Stephanopoulos, J. St-Pierre, D. A. Tennant, C. Wittmann, M. G. V. Heiden, A. Vazquez, K. Vousden, J. D. Young, N. Zamboni, S. M. Fendt, A roadmap for interpreting (13)C metabolite labeling patterns from cells. *Current opinion in biotechnology*. **34**, 189–201 (2015).